Highly active nanostructured palladium-ceria electrocatalysts for the hydrogen oxidation reaction in alkaline medium†

Hamish A. Miller[a*], Francesco Vizza[a*], Marcello Marelli[b], Anicet Zadick[c,d], Laetitia Dubau[c,d], Marian Chatenet[c,d,e], Simon Geiger[f], Serhiy Cherevko[f,g], Huong Doan[h], Ryan K. Pavlicek[h], Sanjeev Mukerjee[h], and Dario R. Dekel[i,j,*]

[a] Istituto di Chimica dei Composti Organometallici (CNR-ICCOM), via Madonna del Piano 10, 50019 Sesto Fiorentino, Firenze, Italy.

[b] Istituto di Scienze e Tecnologie Molecolari (ISTM-CNR) via Camillo Golgi 19, 20133 Milano, Italy.

[c] University of Grenoble Alpes, LEPMI, F-38000 Grenoble, France

[d] CNRS, LEPMI, F-38000 Grenoble, France

[e] French University Institute (IUF), Paris, France

[f] Department of Interface Chemistry and Surface Engineering,Max-Planck-Institut für Eisenforschung GmbH, 40237 Düsseldorf, Germany

[g] Helmholtz-Institute Erlangen-Nürnberg for Renewable Energy (IEK-11), Forschungszentrum Jülich, 91058 Erlangen, Germany

[h] Department of Chemistry and Chemical Biology, Northeastern University, Boston, MA, 02115, USA

[i] The Wolfson Department of Chemical Engineering, Technion – Israel Institute of Technology, Haifa, 3200003, Israel.

[j] The Nancy & Stephan Grand Technion Energy Program (GTEP), Technion – Israel Institute of Technology, Haifa 3200003, Israel.

†Electronic Supplementary Information (ESI) available: [Experimental details and Figs.]. See DOI: 10.1039/b000000x/

Abstract:

We report an interesting new class of bifunctional electrocatalysts, Pd/C-CeO_2, with excellent activity and stability for the hydrogen oxidation reaction (HOR) under alkaline conditions. The unique structure of palladium deposited onto a mixed support of Vulcan XC-72 carbon and CeO_2 consists of Pd metal preferable deposited on the ceria regions of the catalyst. The CeO_2-Pd interaction leads to enhanced HOR kinetics and increased stability. Here we compare catalysts with three different Pd loadings and show that the 10 wt% Pd sample has optimized activity. Hydrogen pumping and fuel cell experiments based on this catalyst show higher activities as compared to a Pd/C sample without ceria. Metal dissolution tests and identical location transmission microscopy experiments show that the catalyst stability under harsh potential cycling experiments in alkaline medium is significantly improved as compared to Pd/C, making this material one of the best options for use as highly active and highly stable electrocatalysts for the HOR in anion exchange membrane fuel cells.

1. Introduction:

Anion exchange membrane fuel cells (AEM-FCs) have received increasing attention as this technology has the potential to replace expensive platinum and platinum alloy materials currently used in fuel cell electrodes, significantly reducing the cost of fuel cell devices.[1] However, the sluggish hydrogen oxidation reaction (HOR) kinetics of electrocatalysts under alkaline conditions have limited the development of affordable Pt-free catalysts and AEM-FC technology is still awaiting new advanced catalytic materials to fulfill its potential.[2] Hence, the realization of a completely Pt-free AEM-FC requires the development of novel anode catalyst structures that enhance the HOR of the supported metal nanoparticles (NPs).[3] A new class of Pd based materials that exploit mixed carbon and metal oxide supports has recently been reported that have led for the first time, performances of non-Pt AEM-FCs with power densities around 0.5 W cm^{-2}, operated with partially filtered air at the cathode and dry hydrogen at the anode.[4] In particular, the addition of CeO_2 to Vulcan XC-72 carbon with a 50:50 weight ratio yields a conductive support onto which Pd deposits preferentially onto the ceria regions (confirmed by EDX-STEM and XAS investigations).[4] When compared to a Pd supported on carbon catalyst (without ceria) with the same particle size distribution and metal loading, a 5-fold improvement is obtained in the anode performance under the same fuel cell conditions for the Pd/C-CeO_2 catalyst. It is believed that the presence of an intimate contact between ceria and Pd enhances the OH^- transfer from the anion conducting membrane and ionomer regions of the fuel cell to the metal surface where the HOR takes place.[5] Cyclic voltammetry (CV) studies have shown a weakening of the Pd-H bonding when ceria is in contact with Pd.[4] The oxidative desorption of hydrogen from Pd (Eqn. 1) is considered to be the rate determining step (rds) of the HOR under alkaline conditions (Eqn. 1).[6, 7]

$$Pd - H + OH^- \rightarrow Pd + H_2O + e^- \quad (1)$$

Hence, a weakening of the bonding of the adsorbed hydrogen can enhance significantly the kinetics. Due to the increasing complexity and challenge of the mechanism of HOR in alkaline media as compared to HOR in acidic medium, the stability of the catalyst is of concern. Due to the scarce data available on HOR catalysts in alkaline medium, stability tests of these materials have not been reported. Specifically for Pd based catalysts, while Pd dissolution in acidic media is well documented,[8, 9] literature data on Pd corrosion in alkaline media is very scarce. Also Pourbaix diagrams, showing stability windows for different species in the E vs. pH space, does not give any

conclusive answer whether Pd corrodes in base. According to a previous report Pd should be extremely stable in typically used alkaline electrolyte.[10] In that report, the authors could not detect any signs of Pd dissolution in 0.5M KOH at 25ºC. However, at alkali concentrations of 6M KOH or higher, and at elevated temperatures some dissolution was detected. Bolzan, interpreting the results obtained using rotating ring disk electrode tests, suggested that some Pd dissolution exists in 1M NaOH, but stressed that the dissolution rates/amounts are significantly lower than that measured in acidic electrolytes.[11] More recently, however, using identical-location transmission electron microscopy (ILTEM) coupled to electrochemistry, Zadick *et al*. demonstrated that the relative stability of Pd towards electrochemical dissolution in base was not a warranty for the stability of state-of-the-art carbon supported Pd nanoparticles at high pH. Indeed, the particles suffer dramatic detachment from their carbon support, overall yielding a very large decrease of electrochemical surface area (ECSA) in a rather limited number of voltammetric cycles (typically below 1000 cycles at 100 mV s^{-1} in the range $0.1 < E < 1.23$ V *vs* RHE) in 0.1 M NaOH at 25°C.[12] Surprisingly, Pt/C nanoparticles were demonstrated to suffer even more such degradation in base electrolytes.[13]

In the present study, we report our continued investigation of the properties of the Pd/C-CeO_2 catalyst, showing its enhanced HOR activity in a hydrogen pumping cell, confirming the ceria effect on the catalytic activity of the Pd. We also report further details on its properties by comparing different Pd ratios on the same C-CeO_2 support (6wt%, 10wt% and 20wt% Pd). Finally, several stability studies of the Pd-C-CeO_2 catalyst are also reported here for the first time, using both *in situ* inductively coupled plasma mass spectrometry (ICP-MS) and identical-location transmission electron microscopy experiments, as well as using hydrogen pumping cells.

2. Experimental

All material manipulations during materials preparation, except as stated otherwise, were routinely performed under nitrogen atmosphere using standard airless technique. Carbon black (Vulcan XC-72 pellets) was purchased from Cabot Corp., USA. All metal salts and reagents were purchased from Aldrich and used as received. All the solutions were freshly prepared with doubly distilled deionized water.

2.1. Material syntheses

2.1.1. Synthesis of Pd/C (10 wt%):

Vulcan XC-72 (6g) was suspended in 250mL of ethylene glycol and sonicated for 20 min in a 500mL three-neck round-bottomed flask. Then an aqueous solution containing H_2O (50mL), ethylene glycol (50mL) and 37% HCl (13mL) with dissolved $PdCl_2$ (1g) was added drop by drop to the Vulcan suspension in a N_2 stream. After adequate stirring, an alkaline solution of NaOH (10.9g) in H_2O (20mL) and ethylene glycol (35mL) was introduced in the reactor and heated at 125^{o}C for 3 hours under a N_2 atmosphere. The mixture was then cooled down to room temperature. The solid product was filtered off and washed with H_2O to neutral pH. The final product was dried in vacuum oven at 65^{o}C. The yield of Pd/C was 6.73g.

2.1.2. Synthesis of C-CeO_2 support (50:50):

Vulcan XC-72 (4g) was added to a solution of $Ce(NO_3)_3.6H_2O$ (10.1g) in H_2O (250 mL). The mixture was kept under stirring for 60 min and sonicated for 30 min. After adjusting the pH to 12 with KOH, the resulting suspension was stirred for 2 hours. The product was separated by filtration and washed with H_2O until neutral pH was obtained. The product was dried at 65^{o}C, then subsequently heated under air in a tube furnace at 250^{o}C for 2 hours. Cooling to room temperature was undertaken under a flow of Ar. The yield of C-CeO_2 was 7.15g.

2.1.3. Synthesis of Pd/C-CeO_2:

The synthetic procedure used was the same for each catalyst with the only difference the amount of Pd salt used to obtain the desired loading of 6wt%Pd, 10wt%Pd and 20wt%Pd. As an example for the 10wt%Pd catalyst, the synthesis was as follows: C-CeO_2 (4g) was suspended in water (500mL), stirred vigorously for 30 min and sonicated for 20 min. To this mixture, a solution of K_2PdCl_4 (1.38g) in water (60mL) was slowly added (during ca. 1 hour) under vigorous stirring, followed by addition of an aqueous solution of 2.5M KOH (8.4mL). Next, ethanol (50mL) was added and the resulting mixture was heated at 80°C for 60 min. The desired product Pd/C-CeO_2 was filtered off, washed several times with distilled water to neutrality and finally dried under vacuum at 65°C until constant weigh was reached. The yield of Pd/C-CeO_2 was 4.45g.

2.2 Electrochemical and physical characterization

Transmission electron microscopy (TEM) was performed on a Philips CM12 microscope at an accelerating voltage of 100kV. The microscope was equipped with an EDAX energy dispersive microanalysis system. Scanning Electron Microscopy (SEM) was performed on a HITACHI S4800

microscope operating at 15kV. High resolution TEM (HR-TEM) images were recorded with a Zeiss Libra 200 FE TEM equipped with a double tilt goniometer at 200kV and FEI Tecnai-F30 microscope which was operated at 300kV. The active metal surface area was determined by CO chemisorption method, adapted to carbon supported materials, at 70°C by the use of an ASAP 2020C Instrument (Micromeritics Corp.). Before the measurements, the samples were reduced at 210°C with H_2 and treated in vacuum at same temperature for 15 hours.

Cyclic Voltammetry (CV) measurements were performed with a Princeton 2273A potentiostat/galvanostat, using a three-electrode arrangement with an Ag/AgCl reference electrode and a platinum foil (25mm x 25mm x 0.1mm) as counter electrode. No IR drop compensation was applied to any of the performed experiments. The potential scale of the CV curves was then converted to the reversible hydrogen electrode (RHE) scale.

Procedures for cell preparation for fuel cell tests are described elsewhere.[4] Cells (5cm^2 active area) consisting in Ag alloy-based cathodes and Pd/C-CeO_2 based anodes with 6wt%Pd, 10wt%Pd, and 20wt%Pd were activated by operating at 50mV in clean air (~10ppm CO_2) (1sLPM, 1barg, dew point 73°C) and dry hydrogen (0.2sLPM, 3barg, room temperature), while heating the cell from room temperature to 73°C. Following temperature and current density stabilization, polarization curves were measured from 50mV to open-circuit at a constant scanning rate of 0.1V min^{-1}.

Hydrogen pump experiments were carried out using 5cm^2 electrodes. For the purposes of these tests, 3 different materials were evaluated as Hydrogen Oxidation Reaction (HOR) catalysts. Commercial Pt/C (46wt%, 3mg_{Pt}/cm^2 + 20% ionomer layer) was used as a standard, while 10wt% Pd/C (0.33mg_{Pd}/cm^2 + 27% ionomer layer) and 10wt%Pd/C-CeO_2 (0.38mg_{Pd}/cm^2 + 30% ionomer layer) were also evaluated. In all cases, Pt/C electrodes identical to the standard were used as CE/RE electrodes for the Hydrogen Evolution Reaction (HER). Electrodes were prepared by spraying an ink solution composed of water, IPA, catalyst, and Nafion onto bare carbon paper supports. An additional topcoat of ionomer was also sprayed onto the electrodes. Prior to use, anion exchange membranes were hydrated for 2 hours in 65°C water, followed by a room temperature solution of 0.5M NaOH for 1 hour to complete the exchange process. The MEA was hot-pressed for 4 minutes under a 3600lb load (100psi) at 60°C.

Testing was done on in-house built test stations, with a cell operating temperature of 60°C with 100% relative humidity. During cell heating and humidification, N_2 was flowed over both electrodes at 100sccm. Anode flow was then switched to H_2 at 100sccm, while the cathode flow remained unchanged.

Stabilization of the MEA was achieved by slowly ramping from 10 to 100mA/cm^2 (10mA/cm^2 increments, 1 minute per step), followed by a 30 minute hold at 100mA/cm^2. Polarization curves were taken from 50 to at least 300mA/cm^2 in 50mA/cm^2 increments, followed by a 1 hour hold at 300mA/cm^2. All measurements were taken on a Metrohm Autolab (PGSTAT302N) paired with a 20A current booster (PGSTAT30). Electrochemical Impedance Spectra (EIS) were taken potentiostatically at the potentials corresponding to the polarization curve current densities.

A modified scanning flow cell (SFC) with a 2mm in diameter opening connected to an inductively coupled plasma mass spectrometer (ICP-MS, NexION, 300X, Perkin Elmer) was used to perform a first set of electrochemical stability tests.[14] The Pd^{106} signal was recorded in relation to the Rh^{103} as an internal standard, which was added downstream of the SFC. The flowrate was 180 µL min^{-1}. All measurements were done in a 0.05M NaOH electrolyte. A glassy carbon plate was employed as the working electrode to support Pd/C-CeO_2 (10wt%Pd) and Pd/C (10wt%Pd) catalysts, while a graphite rod and an Ag/AgCl electrode were used as the counter and reference electrodes, respectively. All potentials are reported against the RHE. For preparation of the catalyst ink 8.5mg of Pd/C-CeO_2 or Pd/C was suspended in 5mL ultrapure water with addition of 20µL Nafion-solution (5wt%, Sigma-Aldrich). After ultrasonic treatment 0.3µL of the suspension were drop-casted on the glassy carbon plate, which after drying, led to the formation of circular spots of ca. 1mm in diameter. The resulting catalyst loading was of 6.5µg$_{Pd}$ cm^{-2}. Afterwards, the carbon plate containing catalyst spots was fixed under the SFC. The catalyst spots were located with the help of a vertical camera attached to the SFC. During measurements the SFC was always placed in such a way that the geometrical centre of the cell and catalyst spot coincided.

Additional stability tests were performed by applying a sequence of CVs in supporting electrolyte at room temperature. The stability procedures used in this study are essentially similar to those used in the literature[12, 13] to monitor the degradation of Pd/C nanoparticles (deposited on the same Vulcan XC72 carbon substrate than here and with a similar loading in Pd). A catalyst ink was prepared by mixing 10mg of Pd/C-CeO_2 catalyst powder, 6.74mL of ultrapure water (18.2MΩ cm, < 3ppb TOC, Elix + Milli-Q Gradient, Millipore), 18.8µL of Nafion® solution (5wt% in water and light alcohols, Electrochem. Inc.®) and 33.9µL of isopropanol. From this ink, 20µL was deposited at a 5 mm-diameter glassy carbon tip, yielding a surface Pd loading of *ca*. 13µgPd cm^{-2}.

The electrochemical experiments were performed in a classical three-electrode cell connected to a VSP numeric potentiostat (Bio-Logic®). The electrolyte was an Ar-purged aqueous solution of 0.1M NaOH at room temperature (T=25°C); this supporting electrolyte was prepared using high-purity reagents (Merck, Suprapur®) and ultrapure water. The counter-electrode was a carbon plate

to avoid pollution issues by metal cations. Hg/HgO was used as reference electrode in the same electrolyte, the potential of which was verified by comparison with a freshly-prepared RHE. All the potential values are nevertheless expressed on the RHE scale. The accelerated stress tests (AST) consisted of 150 and then 1000 CV cycles in the supporting electrolyte, within a potential range of $0.1 < E < 1.23$ V *vs*. RHE; the potential sweep rate was 100mV s^{-1}. During this AST, CV cycles were periodically monitored. The morphology of the Pd/C-CeO_2 nanoparticles was also characterized by identical-location transmission electron microscopy (ILTEM) after 150 and 1000 CV cycles. In that case, the above-mentioned AST was reproduced using a gold + lacey carbon TEM grids as the working electrode. In ILTEM, similar regions of the catalyst are observed before/after the degradation test. The TEM used for these specific characterizations is a JEOL 2010 TEM apparatus, equipped with a LaB6 filament operating at 200 kV (point to point resolution 0.19 Å) and with an Oxford Inca® X-Ray dispersive spectrometer for local chemical analyses.

3. Results and Discussion:

3.1 Material characterization

The XRD diffraction patterns of the as prepared catalyst materials are shown in Figure 1. Trace 1(a) represents the mixed carbon-ceria support and all visible peaks can be assigned to ceria-based reflections. The addition of Pd to the support can be seen by the appearance of a peak at around 40° that can be assigned to Pd metal. The small intensity and broad nature of the peak for these samples is representative of the presence of a large proportion of amorphous Pd oxides in each catalyst as has been confirmed by XAS studies in our previous report.[4] This is particularly obvious when comparing the intensity with that representative of the Pd/C sample (10wt% Pd) in trace (e) where most of the Pd present is metallic. In-situ XRD studies have shown that the Pd oxide in the C-CeO_2 supported samples is reduced metal in the presence of flowing hydrogen.[4]

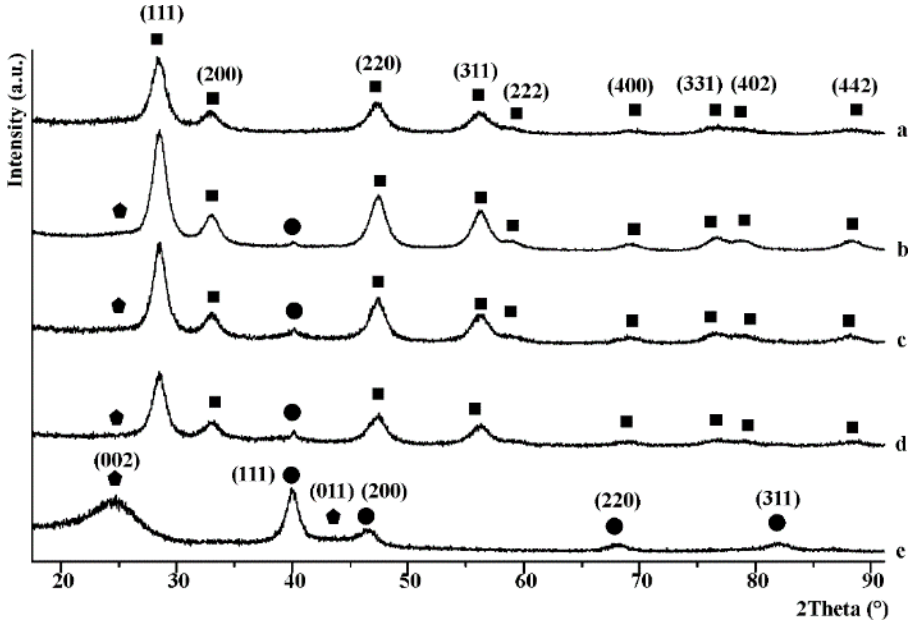

Figure 1. XRD diffraction patterns of (a) 50:50wt% C-CeO_2, (b) Pd/C-CeO_2 (6wt% Pd), (c) Pd/C-CeO_2 (10wt% Pd), (d) Pd/C-CeO_2 (20wt% Pd) and (e) Pd/C (10wt% Pd). Legend: (●) Pd, (■) CeO_2 and (♦) carbon.

The BET data (Table 1) shows that the addition of ceria to Vulcan XC-72 carbon reduces significantly the surface area of the mixed support. At the same time the addition of up to 10wt% Pd to the mixed support does not affect the overall surface area. With 20wt% Pd, the BET surface area drops from around 140 to 124m^2 g^{-1}. Table 1 also shows the active metal (Pd) surface area determined by chemisorption experiments. The data shows a high Pd metal dispersion specific surface area for all samples with a small average calculated particle size. The 10wt% Pd sample shows the highest Pd specific surface area dispersion (236 m^2 g_{Pd}^{-1}) and smallest calculated crystallite size (2.1 nm).

Table 1: Physical characterization data obtained from BET experiments and CO-chemisorption isotherms.

Sample	**BET** $m^2 g^{-1}$	**Catalyst specific surface area** $m^2 g^{-1}_{cat}$	**Metal specific surface area** $m^2 g^{-1}_{Pd}$	**Crystallite size** nm
C (Vulcan XC-72)	222	-	-	-
C-CeO_2 (50wt% CeO_2)	140	-	-	-
Pd/C-CeO_2 (6wt% Pd)	141	9.5	188	2.6
Pd/C-CeO_2 (10wt% Pd)	145	23.6	236	2.1
Pd/C-CeO_2 (20wt% Pd)	124	24.8	146	3.4

To study the catalyst morphology and surface structure, we have found that high resolution Z-contrast STEM is a good technique to elucidate the structure of these catalysts and the Pd metal distribution. In Figure 2, images at different magnifications are shown for the Pd/C-CeO_2 materials with different Pd loadings (6wt%, 10wt% and 20wt% of Pd). Firstly, it can be seen that the CeO_2 particles do not cover uniformly the Vulcan XC-72 carbon material. Some distinct agglomerated CeO_2 structures (brighter structures) can be seen separated from the Vulcan carbon. Pd nanoparticles (NPs) are visible on the bare carbon areas. It is not possible however to individualize Pd NPs on the ceria portions due to poor resolution between these two species. The number of Pd NPs visible on the carbon substrate increases along with the loading. Interestingly, only a few Pd particles are visible on the 6wt% Pd sample (pointed out by arrows). More are visible on the carbon as the metal loading increases and this allows us to determine the average Pd particle size distribution (mean values determined are 2.0nm and 2.5nm for the 10wt% and 20wt% samples, respectively).

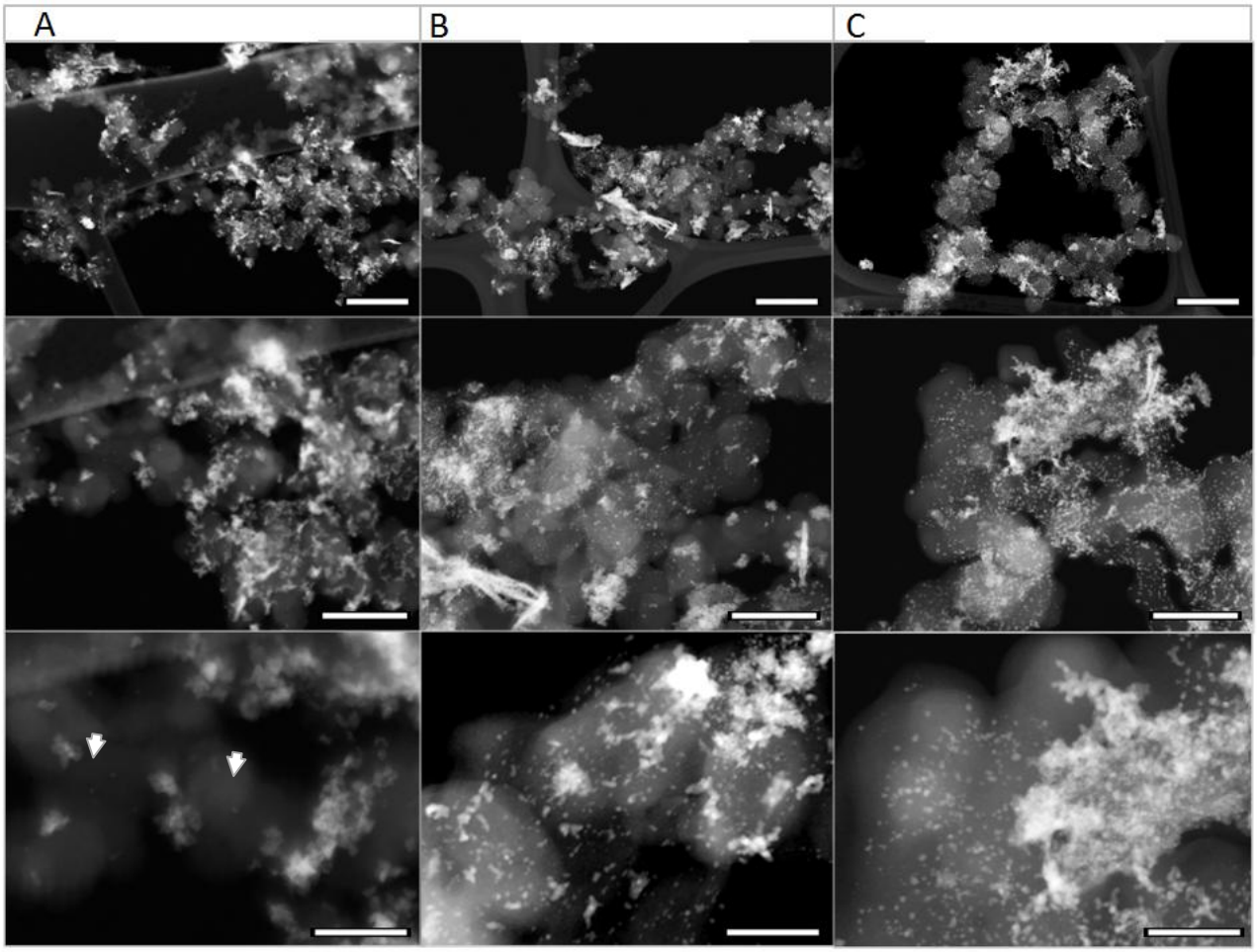

Figure 2: Comparison between the three Pd loadings (A 6%, B 10% and C 20 %) at three different magnifications: scale bar of the first line is 200nm, middle line 100nm and bottom line 50nm.

STEM-EDX analysis can be used to determine the Pd distribution over the whole sample including also the ceria portions of the support. As example, a representative image of the 20wt% Pd sample is shown in Figure 3. Two zones are clearly distinguishable. On the right side a purely carbon portion (in blue) covered with some small Pd NPs (in green). STEM-EDX elemental map analysis shows a large ceria cluster (in red) covering the carbon structure on the left portion of the sample. The Pd mapping shows that although Pd NPs are visible on the carbon section, most of the Pd is deposited on the ceria structures. This trend is consistent with all samples.

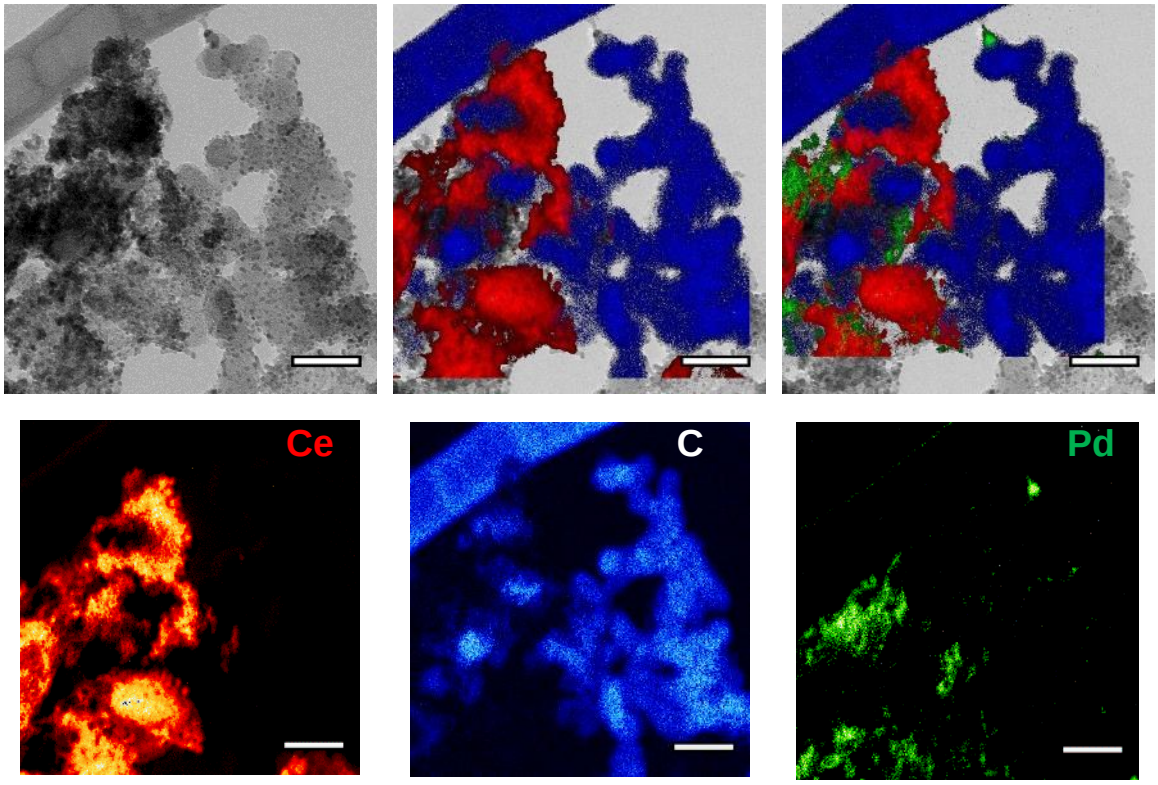

Figure 3: STEM-EDX analysis of a representative portion of the 20wt% Pd catalyst (scale bar 50 nm).

3.2 Electrochemical tests

Electrochemical data are listed in Table 2, including the electrochemically active surface area (ECSA), exchange current densities (i^0) and the mass activity per gram of Pd (i^0, m). The mass activity per gram of Pd is significantly higher for the 10wt% Pd sample relative to both the 6wt% and 20wt% samples. The Tafel analysis of each catalyst, shown in Figure 4, also confirms the increased performance of the 10wt% Pd sample relative to the others. Indeed, increasing the Pd loading from 10% to 20% does not improve the overall activity of the catalyst. Tafel slope analysis reveals a large difference amongst the various catalysts with values of 100, 66 and 143 mV dec^{-1} respectively suggesting a change in the HOR mechanism after a doubling of the Pd loading (10 to 20%). A value of 66 $mVdec^{-1}$ indicates that the rate determining step (rds) for the 10% Pd catalyst is molecular hydrogen dissociative adsorption (Tafel step), while the 20% Pd sample shows a value that suggests charge transfer processes are rate limiting.[7]

Table 2: Electrochemical characterization data.

Pd content in Pd/C-CeO_2 wt%	i_0 $\mu A\ cm_{Pd}^{-2}$	ECSA $m^2\ g^{-1}_{Pd}$	Tafel slope $mV\ dec^{-1}$	$i_{0,m}$ $A\ g_{Pd}^{-2}$
6	89	22	100	19
10	55	43	66	24
20	83	14	143	11

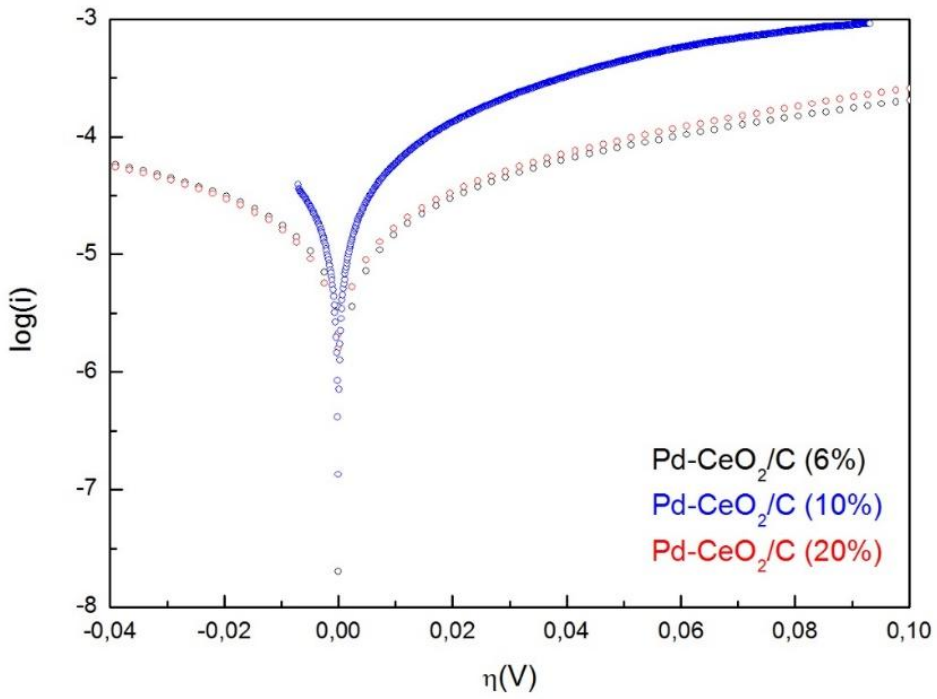

Figure 4. Tafel slope analysis of Pd/C-CeO_2 (6wt%, 10wt% and 20wt% Pd) obtained in H_2-saturated 0.1M KOH at 10mV s^{-1} and 1600rpm.

3.3 Fuel cell tests

For fuel cell tests, the Pd/C-CeO_2 anode catalysts with different Pd concentrations (6wt%, 10wt% and 20wt% Pd) were incorporated into anode catalyst layers (0.15-0.30$mg_{Pd}\ cm^{-2}$). Three identical

cells where the only change was the anode catalyst layer, were prepared for testing in AEM-FC single cells. Figure 5 shows the cell performance at 73 °C run with dry H_2 and filtered air (~10ppm CO_2). Polarization curves of cells with anodes made with Pd/C-CeO_2 (6 and 20wt% Pd) were compared with the previous reported results made with anodes made with Pd/C-CeO_2 10wt% Pd.[4] As can be seen from Figure 5, although results obtained with all catalysts appear to be similar, the Pd/C-CeO_2 10wt% Pd reported previously shows slightly better performance.[4] Table 3 summarizes the fuel cell results.

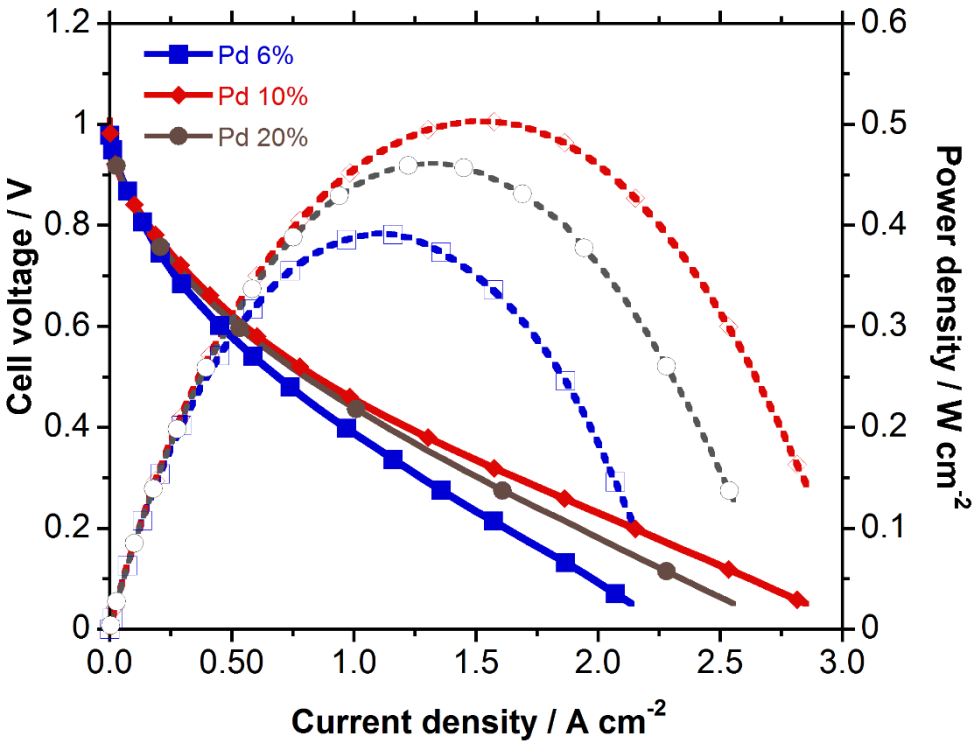

Figure 5. Polarization curves of AEMFCs using Pd/C-CeO_2 anode catalysts with 10wt% Pd,[4] 6%Pd and 20wt%.

Table 3: H_2/air AEM-FC polarization data summary

	Current density at 0.85V mA cm^{-2}	Peak power density mW cm^{-2}
Pd/C-CeO_2 10wt%Pd [[4]]	100	500
Pd/C-CeO_2 6wt%Pd	90	390
Pd/C-CeO_2 20wt%Pd	80	460

As shown in Table 3, the performance of the Pd/C-CeO_2 10wt%Pd catalyst performs slightly better than the other two catalysts with higher and lower Pd loadings. It seems that the high Pd loading (20wt%) does not give any beneficial effect on fuel cell performance, as increasing the amount of Pd from 10wt% to 20wt% leads to more Pd deposited on the carbon regions, as shown in Figure 2. These isolated Pd/C nanoparticles do not contribute to the enhanced activity as they perform as Pd/C, with significantly lower performance due to the lack of the advantage of Pd-ceria interaction.[4]

3.4 Hydrogen pumping tests

Two Pd-based materials were tested in a hydrogen pump system in order to evaluate HOR activity. Once a standard curve of Pt/C was tested, Pd/C and Pd/C-CeO_2 (both 10 %) were evaluated as well. Figure 6 shows the polarization curves from the three materials, demonstrating that the Pd/C-CeO_2 material far outperformed the Pd/C, while showing similar performance to that of a Pt/C anode. This is achieved with a Pd metal loading ~10 times lower than Pt metal loading (0.33mg_{Pd} cm^{-2} vs. 3mg_{Pt} cm^{-2}).

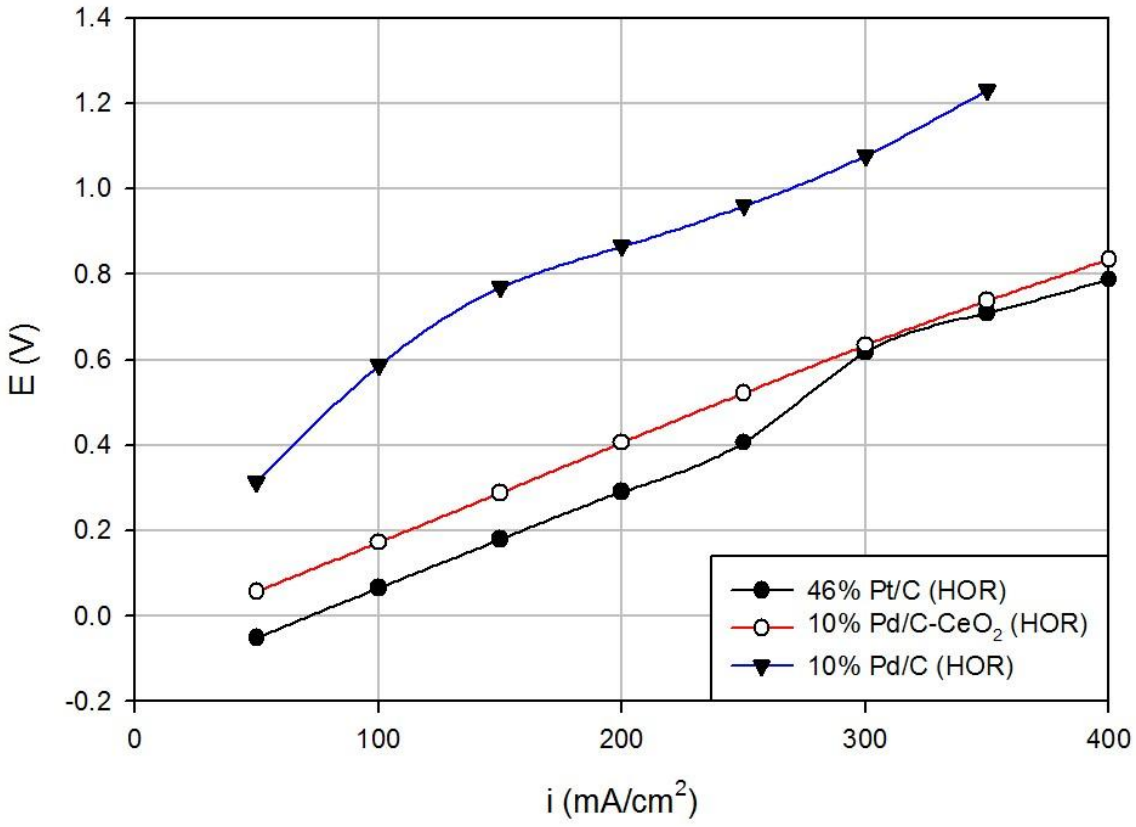

Figure 6. Polarization curves of the hydrogen pumping tests comparing HOR performance of Pd/C-CeO_2 catalyst as compared to both Pd/C as well as Pt/C.

As can be seen, the performance of the Pd/C-CeO_2 catalyst is clearly superior to that obtained with Pd/C. For instance, at 0.4V and 0.8V the current densities obtained with Pd/C-CeO_2 were around three times higher than the current densities obtained with Pd/C. These results confirm the higher activities of Pd/C-CeO_2 as compared to the Pd/C without ceria. Same significantly higher HOR activities of Pd/C-CeO_2 over Pd/C were also shown in fuel cell tests.[4]

Figure 7 shows the steady state performance of a hydrogen pumping cell run at constant 300mA cm^{-2} over the course of 1 hour. While the Pd/C shows an increase in potential during test, Pd/C-CeO_2 catalyst (as well as the Pt/C) shows a very stable performance at a much lower potential. These results indicate that the addition of ceria support to the catalyst improves not just the performance, but also the stability of the catalyst.

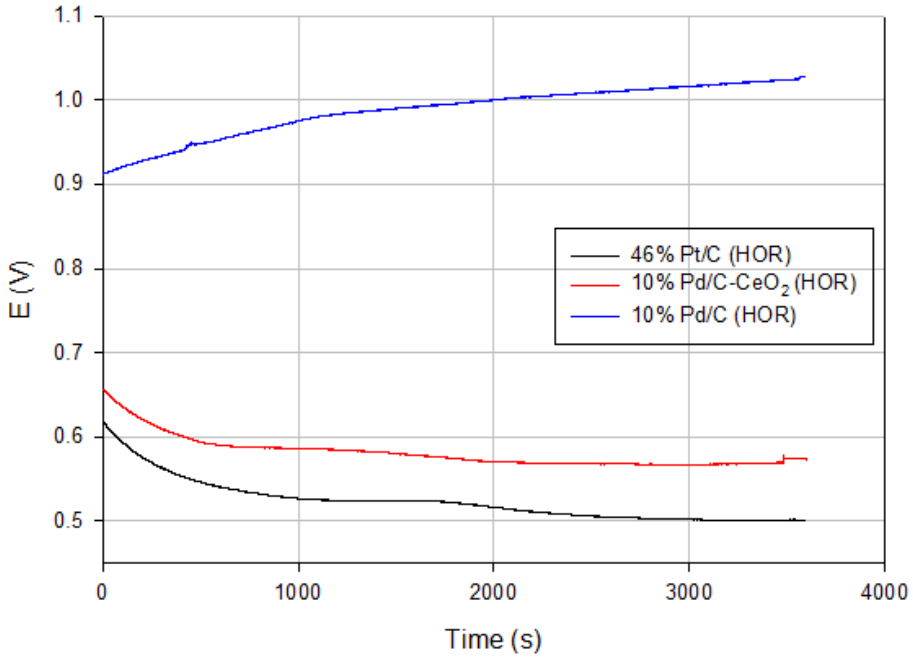

Figure 7. Stability run of hydrogen pumping test of Pd/C-CeO_2 catalyst as compared to both Pd/C and Pt/C under 300mA cm^{-2} steady state operation.

Electrochemical Impedance Spectroscopy (EIS) spectra were taken for all three HOR catalysts. Figure 8 summarizes these results for J = 300mA cm^{-2}. All three materials showed negative shifts in the high-frequency resistance (HFR) as the current density increased. The shift in the Pt/C HFR was significantly larger (~25mΩ) that either the Pd/C (~5mΩ) or the Pd/C-CeO_2 (~15mΩ). The charge transfer resistance (approximated by the distance between to the two y-intercepts) of the Pt/C was less than that of either of the two Pd-based materials. However, the Pd/C-CeO_2 did show an improvement over the Pd/C catalyst. Additionally, the HFR of the Pd/C-CeO_2 catalyst was very similar to that of the Pt/C reference.

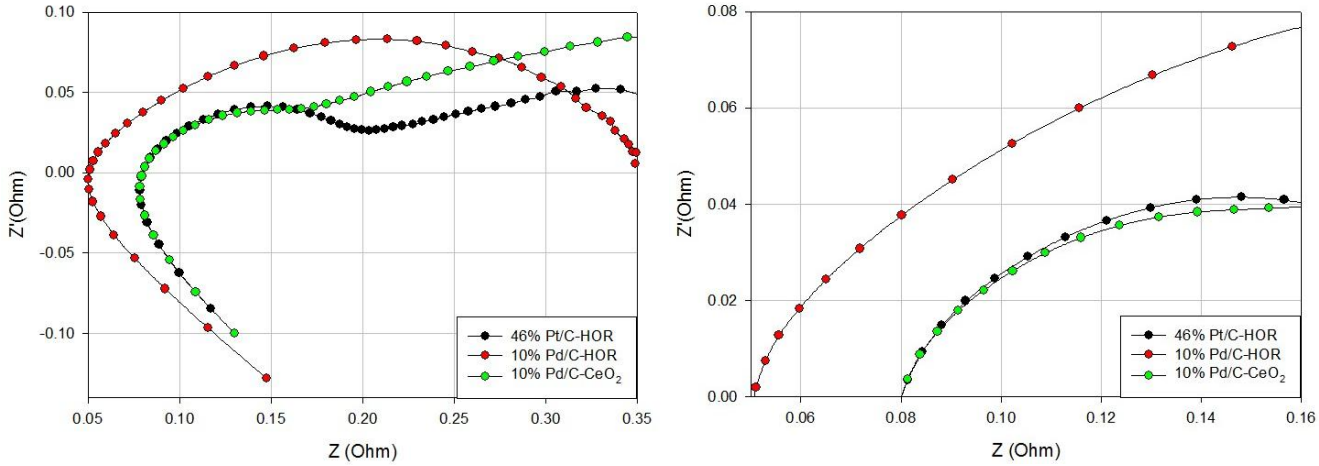

Figure 8. EIS measured during hydrogen pumping tests at current density of 300mA/cm^2. Right plot shows a zoom-in of the left plot.

3.5 Stability tests

To evaluate the catalyst stability of this highly active HOR catalyst, electrochemical tests were performed using a modified SFC to measure the dissolution properties of the 10wt% Pd/C-CeO_2 catalyst in alkaline medium compared to the Pd/C. To get a first insight on the stability of the studied catalysts in alkaline media, CVs in a broad potential window (-0.05 to 1.4 V_{RHE}) of Pd oxide formation and reduction as well as hydrogen sorption and desorption were recorded in Ar-saturated 0.05M NaOH electrolyte. The results are summarized in Figure 9.

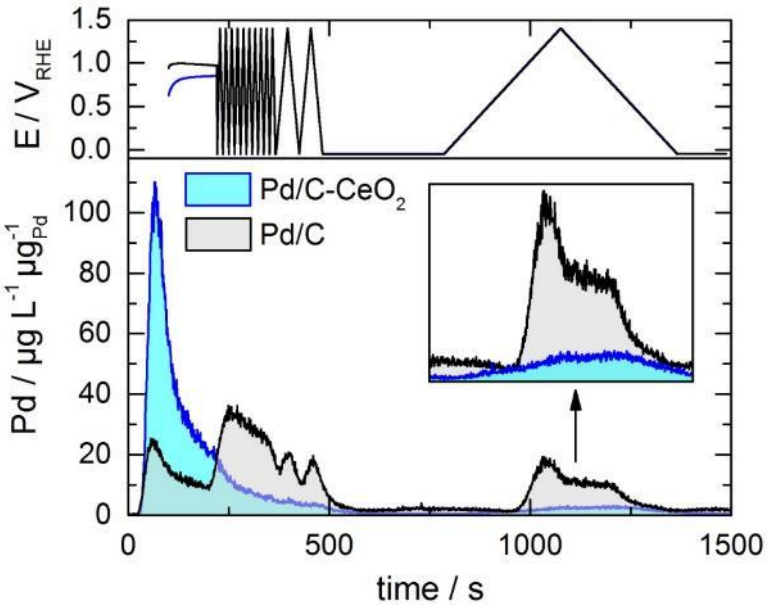

Figure 9. Pd detection profiles of Pd/C and Pd/C-CeO_2 (both 10wt%Pd) during 10 cycles at 200mVs^{-1}, 2 cycles at 50mVs^{-1} and 1 cycle at 5mVs^{-1}, in the range of -0.05 to 1.4 V_{RHE} in 0.05M NaOH purged with Argon.

In Figure 9 the upper pane shows variation of potential with time. This contains a short stay at the open circuit potential (OCV), fast cleaning cycles, two cycles recorded at 50mVs^{-1}, short potentiostating at $-0.05V_{RHE}$, and a slow scan at 5mV s^{-1}. The latter is added for a clear separation between anodic and cathodic dissolution processes, well known for corrosion of other noble metals in acid and base.[15] Dissolution is shown in the lower pane in Figure 9. By comparing the Pd/C-CeO_2 catalyst with Pd/C catalyst one can clearly see that the OCV is slightly lower, while more Pd is detected in this region for Pd/C-CeO_2. This can be an indication of the cathodic dissolution of an unstable Pd oxide, which is consistent with the fact that Pd oxide is found in the Pd/C-CeO_2 catalyst before flowing hydrogen, which reduces the oxide layer to Pd metal (see section 3.1). Since also some cerium dissolution was observed in this region (see Figure S1), it can be assumed that the two processes are related, as it was found that Pd was preferable deposited on ceria regions (see section 3.1). It has to be remarked though, that the observed signal must be due to dissolution but not particle detachments as in the latter case the dissolution rates of Pd and Ce should scale linearly.

From Figure 9 it can be also seen that the Pd/C-CeO_2 catalyst stabilizes with potential cycling, although the detection of Pd by ICP-MS is still non-zero. The contrary is observed for Pd/C where Pd detection from this electrode significantly increases with potential cycling. The origin of the detection of Pd can here originate both from dissolution of the Pd nanoparticles or from their

detachment from the carbon support, the latter having been found non-negligible in NaOH electrolytes by ILTEM experiments.[12] The total amount of Pd lost from both electrodes during the OCV and the potential cycling is ca. 1.4ng, which is 3% of the initial loading. Both electrodes are stabilized during the following potential step at −0.05 V_{RHE}. When potentials move into anodic direction, Pd starts to dissolve from both electrodes. Interestingly, the onset of Pd dissolution from Pd/C-CeO_2 is significantly lower that for Pd/C (see inset in Figure 9), suggesting a different mechanism (or different kinetics) of Pd loss. Even if initiated later, Pd/C dissolution however, shows much higher dissolution rates (up to an order of magnitude) at the higher potentials. At even higher potentials Pd passivates, likely due to formation of a stable oxide. Some increase in dissolution is also observed during oxide reduction, although the amounts are lower. As previously indicated, the reason for the superior stability of Pd/C-CeO_2 may be a strong Pd-ceria interaction. It can also be that in Pd/C-CeO_2, most of the Pd nanoparticles are supported on the CeO_2 (and not on carbon), and are therefore not subjected to the harsh nanoparticle detachment that occurs for carbon-supported Pd/C nanoparticles. This hypothesis will be explored by ILTEM experiments (see below).

It is anticipated that during normal operation of an AEM-FC the highest anodic potential the anode will experience is the potential at open circuit (0.9V-1.0V vs RHE), which is significantly lower than the upper potential limit of cycling used in the experiments presented in Figure 9 (=1.4V vs RHE). Also, as hydrogen can influence (reduce) the Pd oxide layer of the Pd/C-CeO_2 catalyst, a second protocol shown in Figure 10 was used to investigate Pd stability at much realistic conditions (better simulating an AEM-FC environment). In this case, the upper potential limit was moved to 1.0 V_{RHE} and the cleaning cycles were excluded. Moreover, dissolution was studied in argon as well as in hydrogen, to test if hydrogen influences stability and to see if the improved activity of Pd/C-CeO_2 towards HOR holds also in SFC tests.

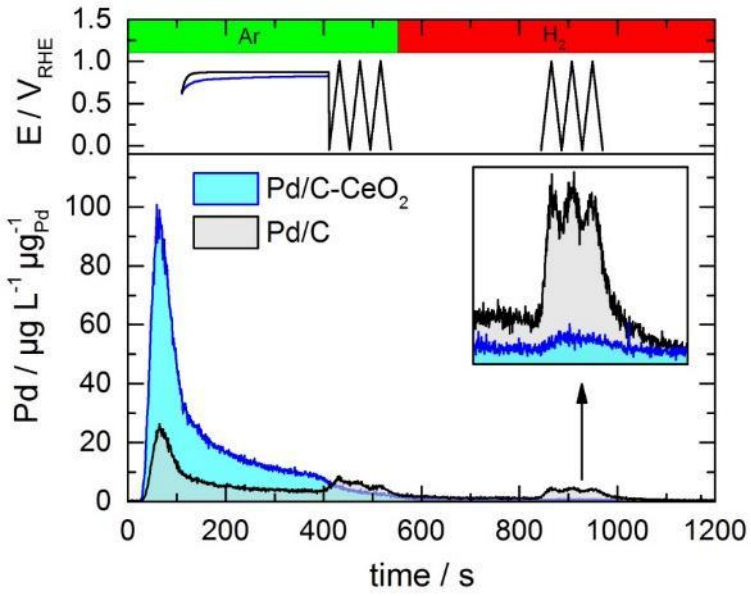

Figure 10. Dissolution profiles of Pd/C and Pd/C-CeO_2 (10wt%Pd) during cycling at 50mV s^{-1} in the range of −0.05 to 1.0 V_{RHE} in 0.05M NaOH purged with argon (in first, green left area) and then with hydrogen (in second, red right area).

For both electrodes, the dissolution behavior during the OCV and potential cycling in argon is analogous to that discussed above. Furthermore, no significant difference was observed when the gas was switched to hydrogen. In hydrogen, Pd behaves similarly to Pt in acid.[16] The inset in Figure 10 presents a magnified view of the dissolution profile, where it can be clearly seen that the amount of Pd dissolved from Pd/C-CeO_2 is significantly lower as compared to that dissolved from Pd/C, indicating that the stability of the Pd/C-CeO_2 is remarkable higher than the stability of Pd/C. In this region, the estimated amount of dissolved Pd was 50pg and 5pg for Pd/C and Pd/C-CeO_2, respectively. Hence, assuming that dissolution rate is not changing with material consumption (a very rough estimation) all Pd should be completely dissolved in 3000 and 30000 cycles up to 1.0 V_{RHE} from the Pd/C and Pd/C-CeO_2 electrodes, respectively. These results suggest that the excellent stability of the Pd/C-CeO_2 may be related to the Pd-ceria interaction.

To further examine the stability of the Pd/C-CeO_2 catalyst and investigate the mechanisms of degradation of these materials, CV cycling tests were also performed and analyzed. Figure 11 presents a sequence of CVs obtained on the Pd/C-CeO_2 (10wt%Pd) catalyst upon aging in 0.1 M NaOH (at 25°C) supporting electrolyte. It can be seen that the overall shape of the CV is very similar to that obtained on the same material in 0.1M KOH, previously reported,[4] although in that latter case, the peak related to Pd-oxides reduction was more pronounced, because the upper vertex

potential was larger (1.3V *vs.* RHE instead of 1.4 V *vs.* RHE) and the scan rate value was lower. One also clearly sees that the signature of Pd-hydrides and Pd-oxides gradually level off upon cycling.

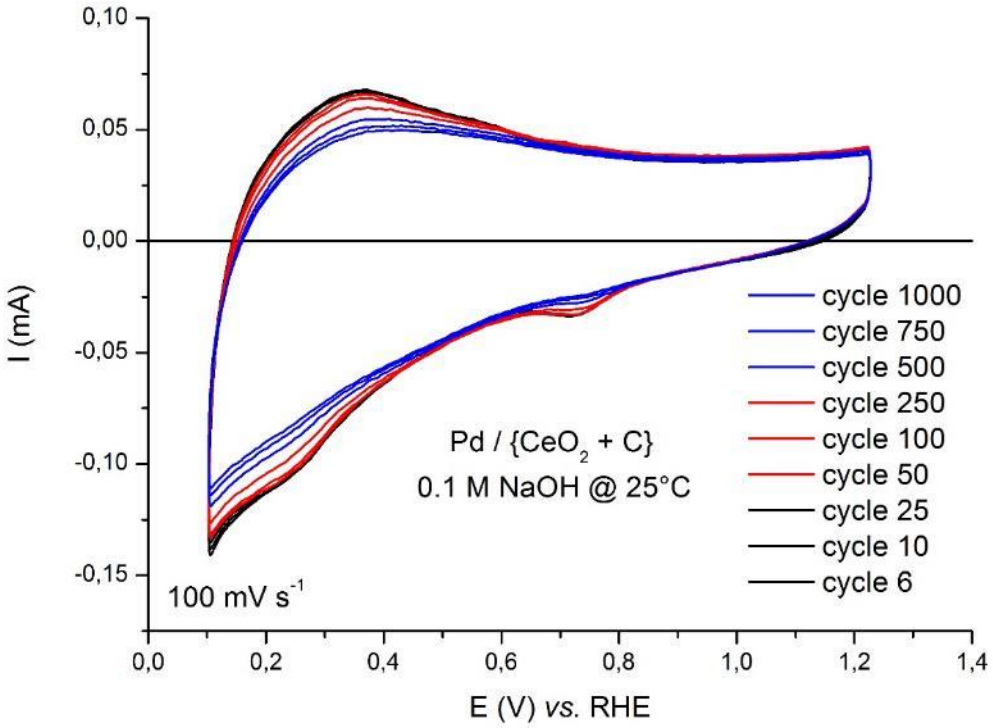

Figure 11. CVs monitored on the Pd/C-CeO_2 (10wt%Pd) catalyst upon aging in 0.1M NaOH supporting electrolyte at 25°C.

To complement the electrochemical experiments, ILTEM micrographs were acquired for Pd/C-CeO_2 after 150 and 1000 CV cycles (Figure 13) and for comparison, ILTEM micrographs of the Pd/C sample in its pristine state, and after 1000 CV are shown in Figure 12. For Pd/C (and this has been observed in a similar manner for "large" and "small" nanoparticles of Pd/C,[12, 13] more than 50% of the Pd nanoparticles were lost in the experiment, probably due to detachment of the nanoparticles from the carbon substrate (Figure 12). Further stability tests are needed to clearly determine whether detachment of the particles actually occurs. Figure 13 shows for the same aging test with Pd/C-CeO_2, that no major loss of Pd nanoparticles is observed, even after 1000 CV cycles.

In the case of the Pd/C-CeO_2 nanoparticles, the mechanisms at stake in the degradation test are completely different than for Pd/C. The micrographs of Figure 13 indeed show no consequent

detachment of nanoparticles, but instead, their shape is progressively and severely modified upon cycling. Whereas the Pd crystallites of Pd/C-CeO_2 were (agglomerated but) small initially (*ca.* 2.1 nm in diameter,[12] they grow after 150 and especially 1000 CV cycles in supporting electrolyte. After 1000 CV, the originally agglomerated, small, and ill-defined Pd nanoparticles (all these observations agree with the results of XRD, CO-chemisorption and SEM/TEM presented above) are transformed into much larger and round-shape (for most of them) single crystalline nanoparticles (Figure 13). This process is a clear coalescence of the Pd nanoparticles initially present within agglomerates, probably according to a dissolution/redisposition mechanism on a short distance scale. It is worth noting that no new nanoparticles are created by the degradation, which rules out massive random redisposition, and the change of shape of isolated (not initially agglomerated) nanoparticles is very minimal, ruling out the *usual* 3D Ostwald ripening mechanism at long scale. In addition, it seems that when the Pd nanoparticles were initially not agglomerated (isolated), they remained isolated afterwards, and that the extent of detachment is much less than observed for a Pd/C sample (see Zadick et al.[13] and Figure 12). This is particularly obvious on the selected micrographs of Figure 14.

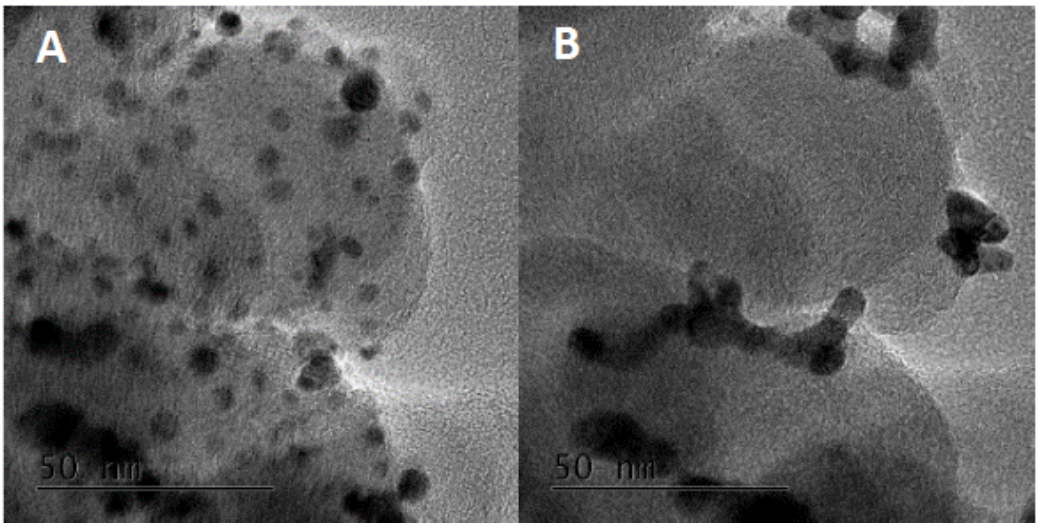

Figure 12. Selected ILTEM micrographs of the Pd/C sample in (A) its pristine state, and (B) after 1000 CV cycles in 0.1M NaOH at 25°C.

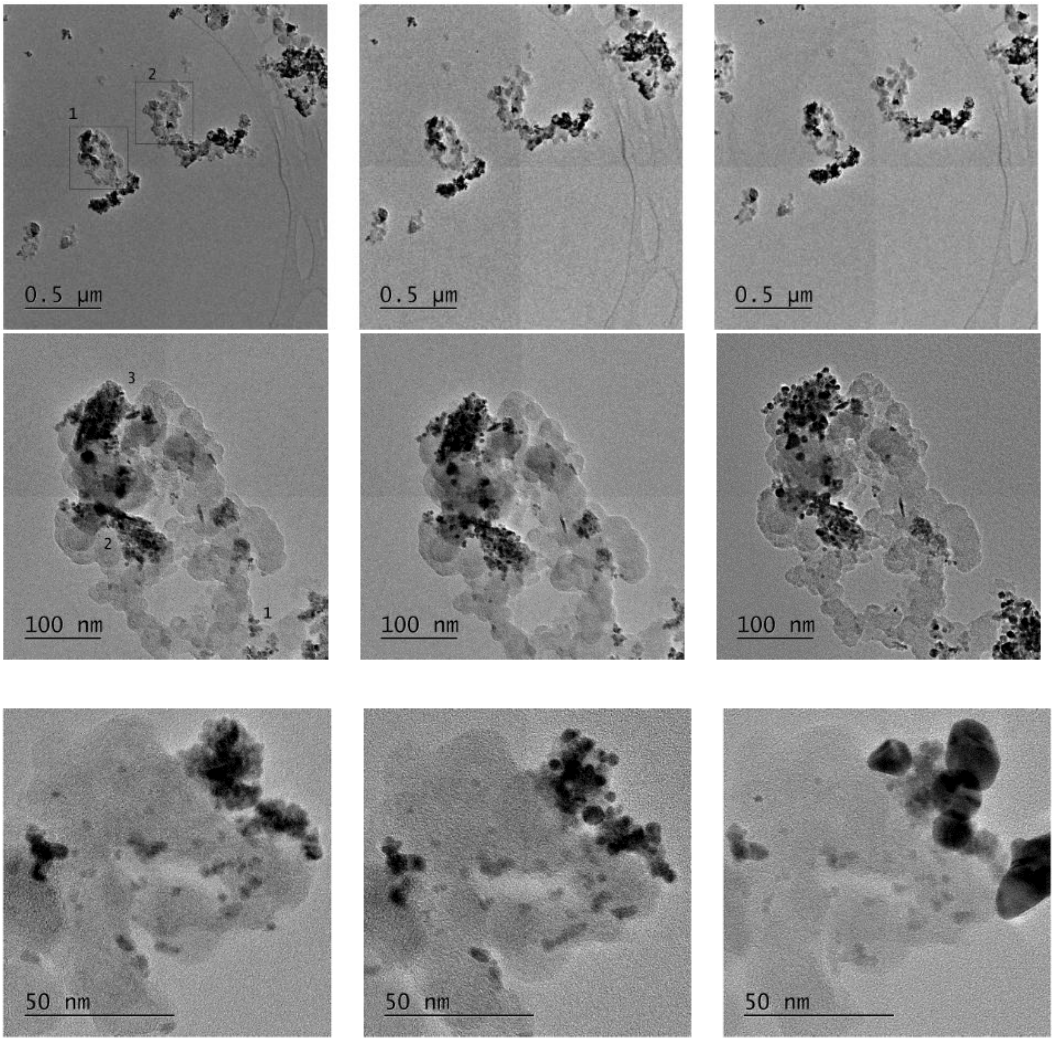

Figure 13 ILTEM micrographs of the Pd/C-CeO_2 sample in its pristine state (left), and after 150 (center) and then 1000 CV (right) cycles in 0.1M NaOH at 25°C. Although the vast majority of the Pd/C-CeO_2 nanoparticles undergo extensive agglomeration/coalescence (top micrographs), some (very few) regions are subjected to much less growth of the Pd crystallites and are subjected to (minor) loss of Pd nanoparticles (bottom micrographs).

In summary from ILTEM and CV aging studies, we can also say that the Pd/C-CeO_2 sample is much more stable in these operating conditions than its Pd/C counterpart. It is likely that the strong interaction of Pd with the CeO_2 and the related "more oxidized" state of Pd atoms do have a favorable impact on the durability of the Pd nanoparticles.[4] In addition, as most of the Pd nanoparticles in Pd/C-CeO_2 are in the vicinity of the CeO_2, the latter being previously coated onto the Vulcan carbon, it can be speculated that the Pd nanoparticles in Pd/C-CeO_2 are mostly not in

direct contact with the surface of the Vulcan carbon, as demonstrated in the high-resolution images of Figure 14. This hypothesis is also in agreement with the pronounced decrease of the BET area of the CeO_2-coated Vulcan versus the pure Vulcan carbon (see section 3.1), which is compatible with the coating of the latter and related coverage/plugging of the micropores inside the carbon particles.

As it is precisely the interface of the Pd with carbon which is believed to be altered upon AST for the Pd/C samples (see Figure 12),[12] one may understand why the Pd/C-CeO_2 sample is more robust than Pd/C in terms of particle detachment. However, this robustness is not a guaranty of complete stability, since instead of particle detachment; the agglomerates of Pd nanoparticles supported on the C-CeO_2 substrate suffer extensive coalescence into larger nanoparticles. This extensive dissolution/redisposition essentially proceeds at short distance scale (essentially inside existing agglomerates but not from groups of nanoparticles separated by several 10nm or more), as illustrated in Figure 13. Figure 14 shows another remarkable example of such processes; in this case, the HRTEM images show that the grown Pd nanoparticle is clearly supported on CeO_2 crystals and not directly on the carbon substrate.

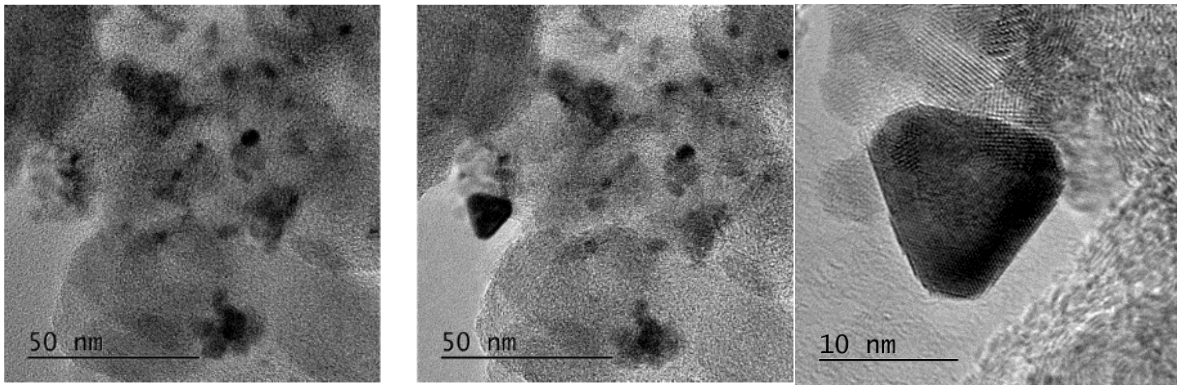

Figure 14. High-magnification micrographs of a grown monocrystalline Pd nanoparticle in contact with several smaller CeO_2 nanoparticles, for the Pd/C-CeO_2 catalyst; pristine (left), and after 1000 cycles (middle and right).

It can be pointed out that such dissolution/redisposition at short range agrees with the ICP-MS findings of Figure 9 and Figure 10; such a process has also already been witnessed for unsupported Pd nanocubes.[17] Two hypotheses can be put forth to account for the different mechanisms of degradation of the Pd nanoparticles in Pd/C and Pd/C-CeO_2: on the one hand, the fate of large Pd ensembles (agglomerates, more present in the initial Pd/C-CeO_2 sample than in the Pd/C ones previously[12] tested could differ from that of isolated Pd because (i) the proximity between

individual crystallites in agglomerates could favor short-scale dissolution/redisposition of Pd or (ii) these large ensembles could have more anchoring points to the substrate. On the other hand, as previously hypothesized, it can be that the stability of the Pd/C-CeO_2 nanoparticles are uniquely linked to the proximity of Pd to the CeO_2 phase (anchoring points of the Pd nanoparticles to the Vulcan carbon (see Figure 12), which are prone to destruction in these conditions, are replaced by tougher anchoring points to the CeO_2 surface, see Figure 14), again in agreement with the findings of ICP-MS. More studies are necessary to understand precisely the mechanisms of degradation of these materials, but this does not put into question the much enhanced durability of the Pd/C-CeO_2 nanoparticles noted here compared to Pd/C catalysts.

Conclusions

We report a new class of bifunctional electrocatalyst for the hydrogen oxidation reaction in fuel cells under alkaline conditions. The electrocatalysts, denoted Pd/C-CeO_2, consist of deposited Pd nanoparticles on a support mixture of 50:50 carbon and CeO_2. The Pd is preferentially deposited on the ceria regions of the support. Previous reports on AEM-FCs as well as the hydrogen pump tests described in this report show that the Pd/C-CeO_2 catalyst has significantly higher activity than Pd/C towards the HOR in alkaline medium. Indeed the activity is similar to that of Pt/C under hydrogen pump experimental conditions. In addition, we have performed preliminary stability studies on Pd/C-CeO_2 showing that catalyst stability under harsh potential cycling is improved as compared to Pd/C. To the best of our understanding, the Pd/C-CeO_2 bifunctional material studied in this report is the HOR electrocatalyst with highest activity and stability for AEM-FCs so far developed.

Acknowledgements

We acknowledge the Ente Cassa di Risparmio di Firenze ITALY (projects HYDROLAB2 and EnergyLab) for financial support.

References

[1] J.R. Varcoe, P. Atanassov, D.R. Dekel, A.M. Herring, M.A. Hickner, P.A. Kohl, A.R. Kucernak, W.E. Mustain, K. Nijmeijer, K. Scott, T.W. Xu, L. Zhuang, Anion-exchange membranes in electrochemical energy systems, Energ Environ Sci, 7 (2014) 3135-3191.

[2] J. Durst, A. Siebel, C. Simon, F. Hasche, J. Herranz, H.A. Gasteiger, New insights into the electrochemical hydrogen oxidation and evolution reaction mechanism, Energ Environ Sci, 7 (2014) 2255-2260.

[3] M. Alesker, M. Page, M. Shviro, Y. Paska, G. Gershinsky, D.R. Dekel, D. Zitoun, Palladium/nickel bifunctional electrocatalyst for hydrogen oxidation reaction in alkaline membrane fuel cell, J Power Sources, 304 (2016) 332-339.

[4] H.A. Miller, A. Lavacchi, F. Vizza, M. Marelli, F. Di Benedetto, F.D.I. Acapito, Y. Paska, M. Page, D.R. Dekel, A Pd/C-CeO2 Anode Catalyst for High-Performance Platinum-Free Anion Exchange Membrane Fuel Cells, Angew Chem Int Edit, 55 (2016) 6004-6007.

[5] D. Strmcnik, M. Uchimura, C. Wang, R. Subbaraman, N. Danilovic, D. van der Vliet, A.P. Paulikas, V.R. Stamenkovic, N.M. Markovic, Improving the hydrogen oxidation reaction rate by promotion of hydroxyl adsorption, Nat Chem, 5 (2013) 300-306.

[6] Y. Wang, G.W. Wang, G.W. Li, B. Huang, J. Pan, Q. Liu, J.J. Han, L. Xiao, J.T. Lu, L. Zhuang, Pt-Ru catalyzed hydrogen oxidation in alkaline media: oxophilic effect or electronic effect?, Energ Environ Sci, 8 (2015) 177-181.

[7] S. St John, R.W. Atkinson, R.R. Unocic, T.A. Zawodzinski, A.B. Papandrew, Ruthenium-Alloy Electrocatalysts with Tunable Hydrogen Oxidation Kinetics in Alkaline Electrolyte, J Phys Chem C, 119 (2015) 13481-13487.

[8] S. Cherevko, A.R. Zeradjanin, A.A. Topalov, N. Kulyk, I. Katsounaros, K.J.J. Mayrhofer, Dissolution of Noble Metals during Oxygen Evolution in Acidic Media, Chemcatchem, 6 (2014) 2219-2223.

[9] B.R. Shrestha, A. Nishikata, T. Tsuru, Channel flow double electrode study on palladium dissolution during potential cycling in sulfuric acid solution, Electrochim Acta, 70 (2012) 42-49.

[10] J.F. Llopis, Gamboa,J.M., and Victori L., Electrochim Acta, 17 (1972) 2225-2230.

[11] A.E. Bolzan, Phenomenological Aspects Related to the Electrochemical-Behavior of Smooth Palladium Electrodes in Alkaline-Solutions, J Electroanal Chem, 380 (1995) 127-138.

[12] A. Zadick, L. Dubau, U.B. Demirci, M. Chatenet, Effects of Pd Nanoparticle Size and Solution Reducer Strength on Pd/C Electrocatalyst Stability in Alkaline Electrolyte, J Electrochem Soc, 163 (2016) F781-F787.

[13] A. Zadick, L. Dubau, N. Sergent, G. Berthome, M. Chatenet, Huge Instability of Pt/C Catalysts in Alkaline Medium, Acs Catal, 5 (2015) 4819-4824.

[14] S.O. Klemm, A.A. Topalov, C.A. Laska, K.J.J. Mayrhofer, Coupling of a high throughput microelectrochemical cell with online multielemental trace analysis by ICP-MS, Electrochem Commun, 13 (2011) 1533-1535.

[15] S. Cherevko, A.R. Zeradjanin, G.P. Keeley, K.J.J. Mayrhofer, A Comparative Study on Gold and Platinum Dissolution in Acidic and Alkaline Media, J Electrochem Soc, 161 (2014) H822-H830.

[16] A.A. Topalov, A.R. Zeradjanin, S. Cherevko, K.J.J. Mayrhofer, The impact of dissolved reactive gases on platinum dissolution in acidic media, Electrochem Commun, 40 (2014) 49-53.

[17] A. Zadick, L. Dubau, A. Zalineeva, C. Coutanceau, M. Chatenet, When cubic nanoparticles get spherical: An Identical Location Transmission Electron Microscopy case study with Pd in alkaline media, Electrochem Commun, 48 (2014) 1-4.

Table 1

Table 1: Physical characterization data obtained from BET experiments and CO-chemisorption isotherms.

Sample	**BET** $m^2 g^{-1}$	**Catalyst specific surface area** $m^2 g^{-1}_{cat}$	**Metal specific surface area** $m^2 g^{-1}_{Pd}$	**Crystallite size** **nm**
C (Vulcan XC-72)	222	-	-	-
C-CeO_2 (50wt% CeO_2)	140	-	-	-
Pd/C-CeO_2 (6wt% Pd)	141	9.5	188	2.6
Pd/C-CeO_2 (10wt% Pd)	145	23.6	236	2.1
Pd/C-CeO_2 (20wt% Pd)	124	24.8	146	3.4

Table 2

Table 2: Electrochemical characterization data.

Pd content in Pd/C-CeO_2 wt%	i_0 $\mu A\ cm_{Pd}^{-2}$	ECSA $m^2\ g^{-1}_{Pd}$	Tafel slope $mV\ dec^{-1}$	$i_{0,m}$ $A\ g_{Pd}^{-2}$
6	89	22	100	19
10	55	43	66	24
20	83	14	143	11

Table 3

Table 3: H_2/air AEM-FC polarization data summary

	Current density at 0.85V mA cm^{-2}	Peak power density mW cm^{-2}
Pd/C-CeO_2 10wt%Pd [[4]]	100	500
Pd/C-CeO_2 6wt%Pd	90	390
Pd/C-CeO_2 20wt%Pd	80	460

Figure 1

Click here to download high resolution image

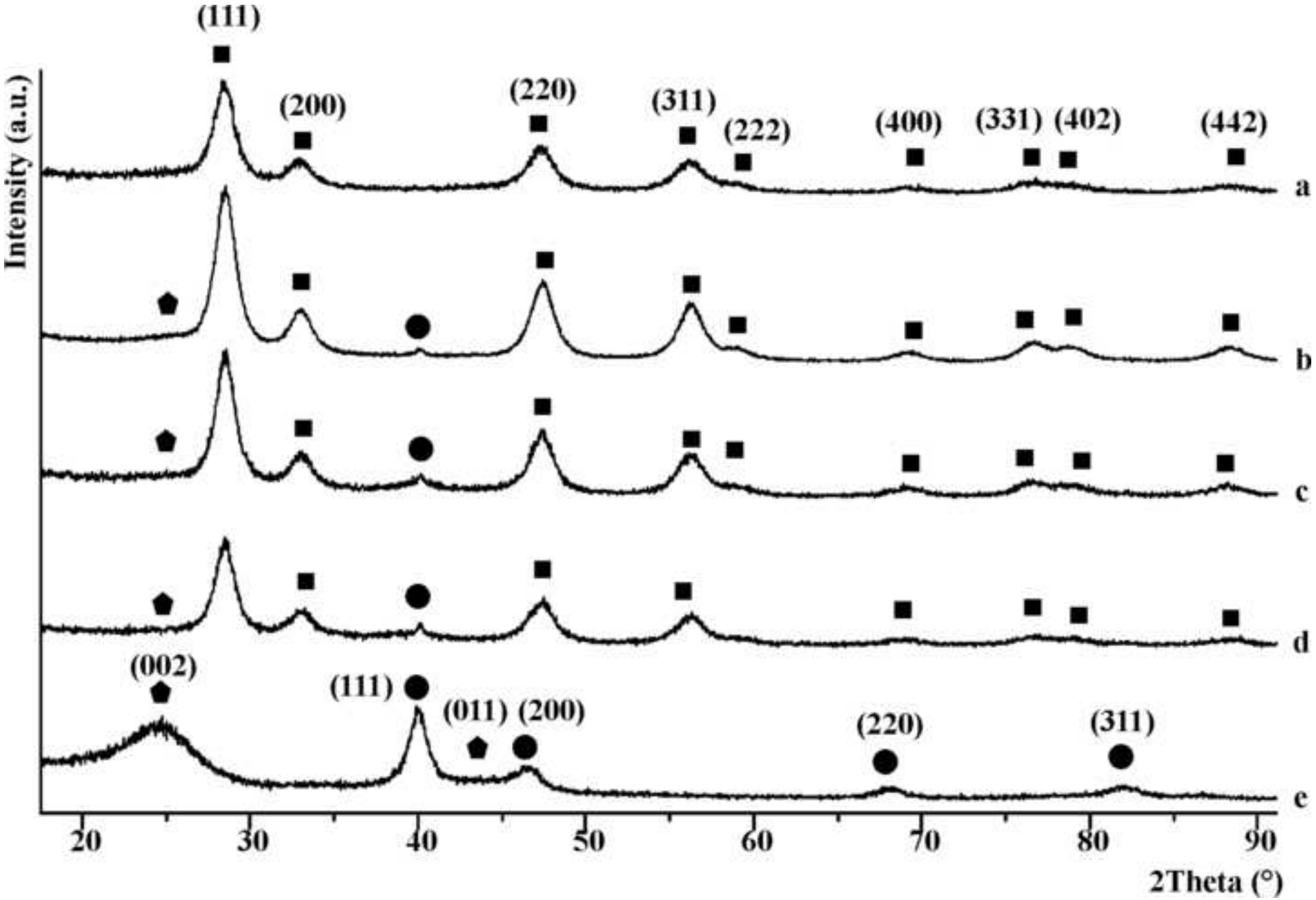

Figure 2

Click here to download high resolution image

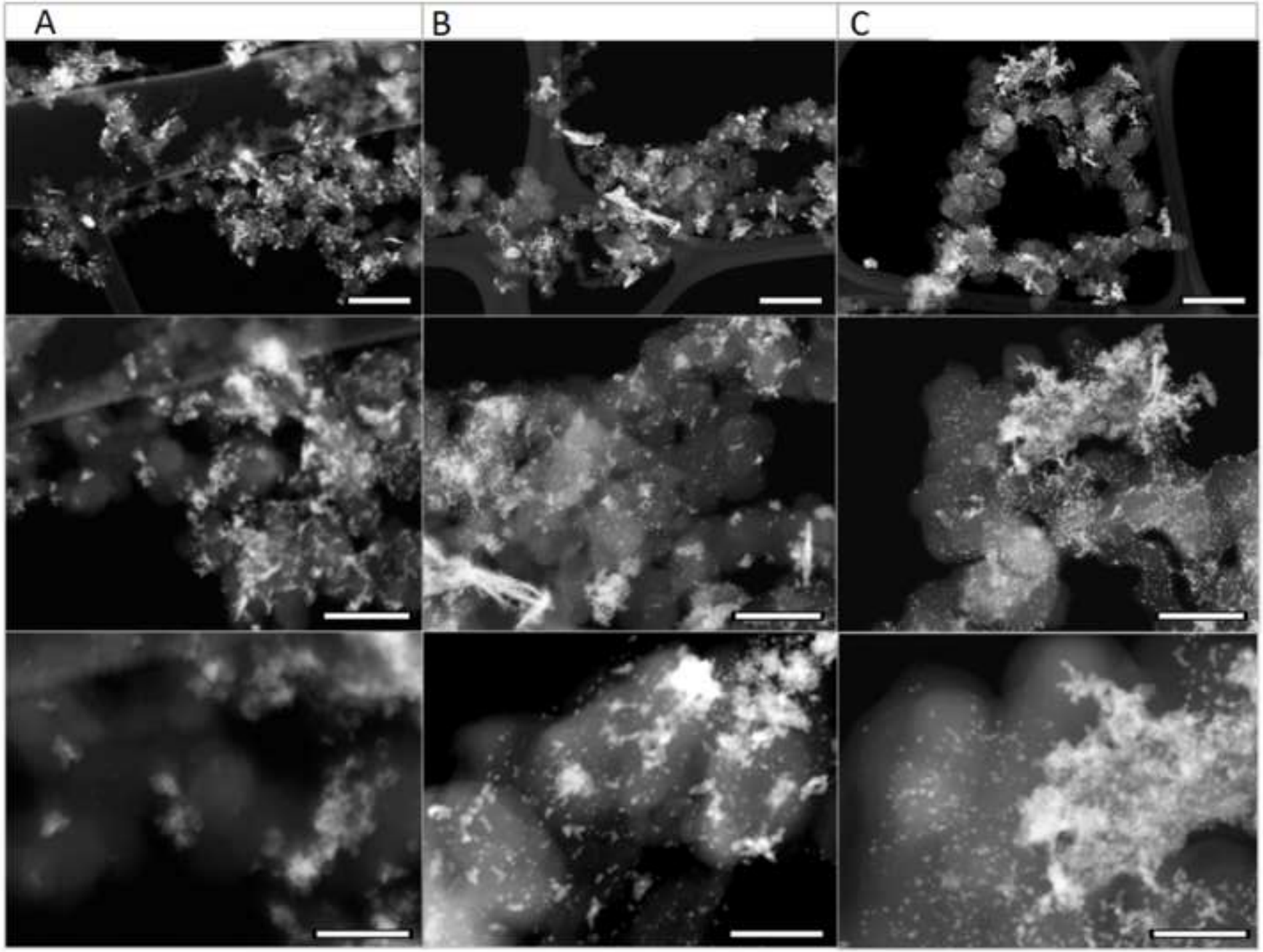

Figure 3

Click here to download high resolution image

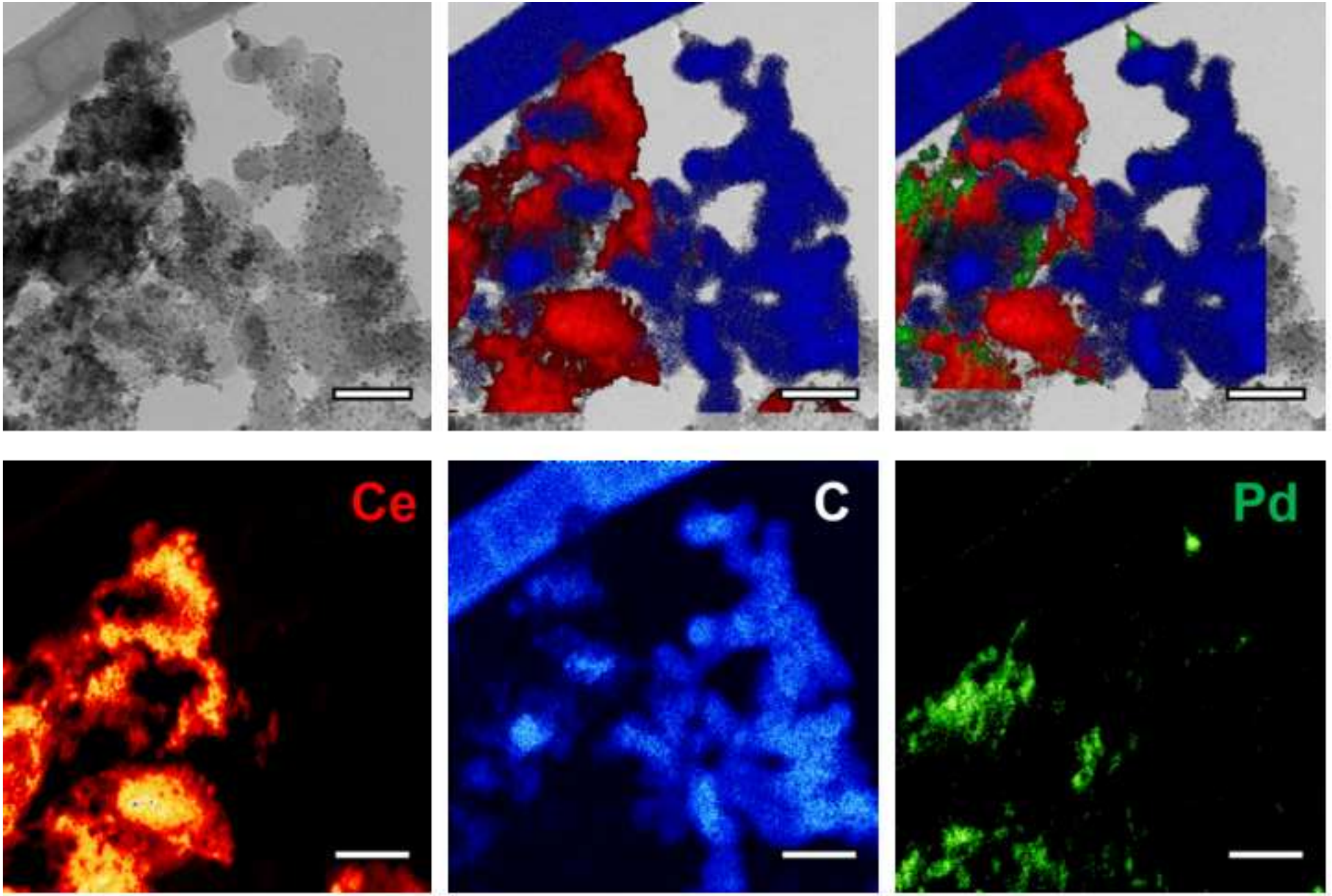

Figure 4

Click here to download high resolution image

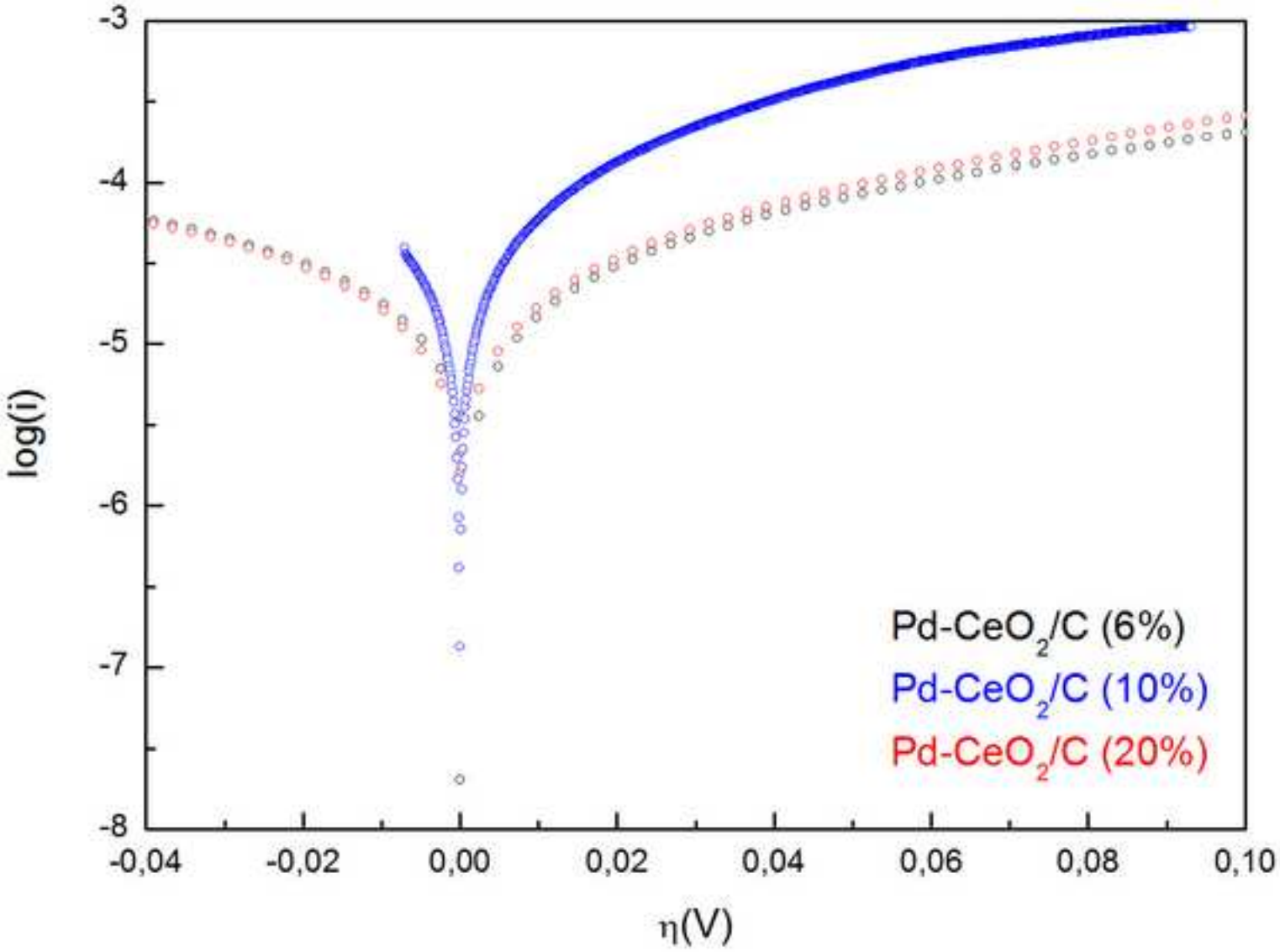

Figure 5

Click here to download high resolution image

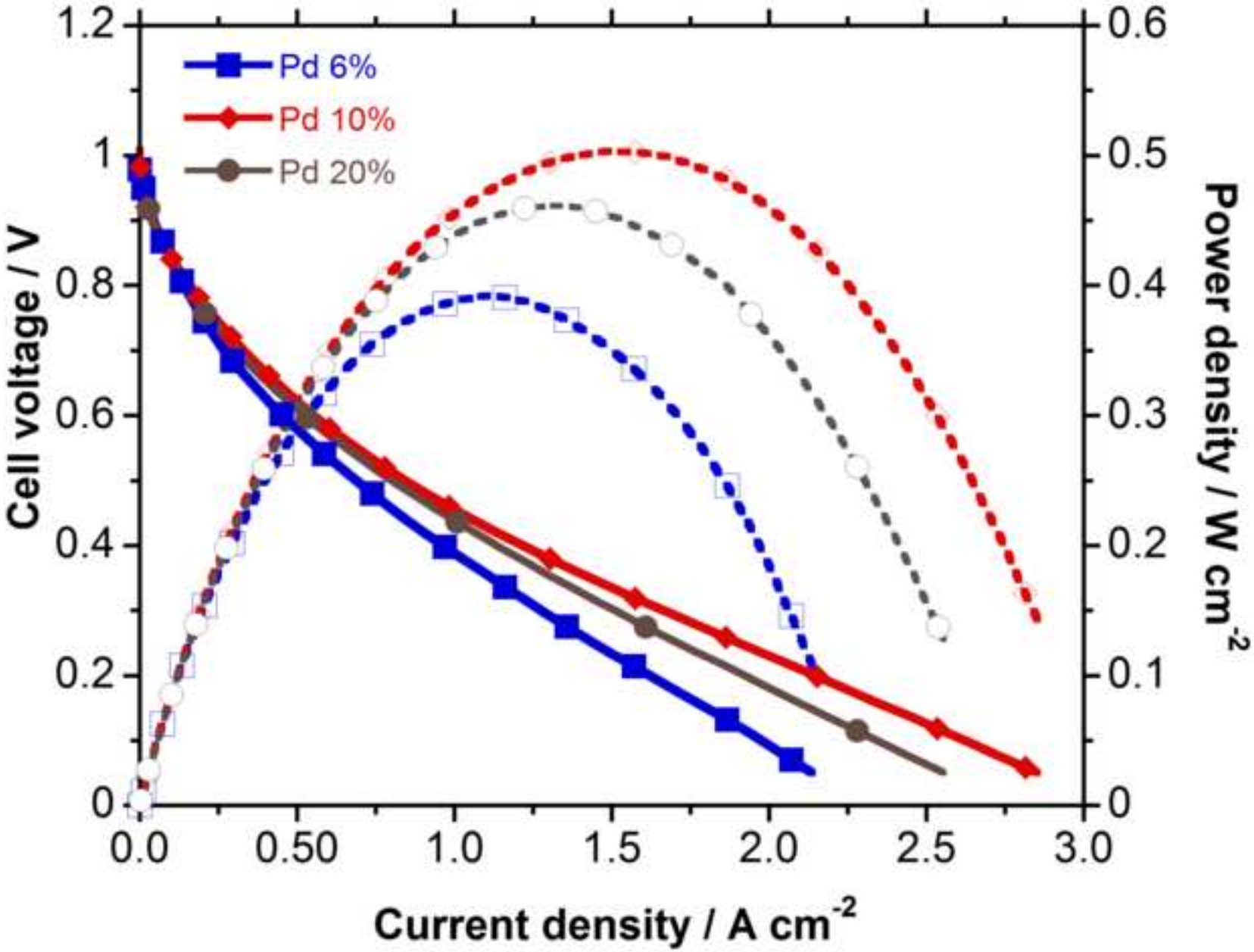

Figure 6

Click here to download high resolution image

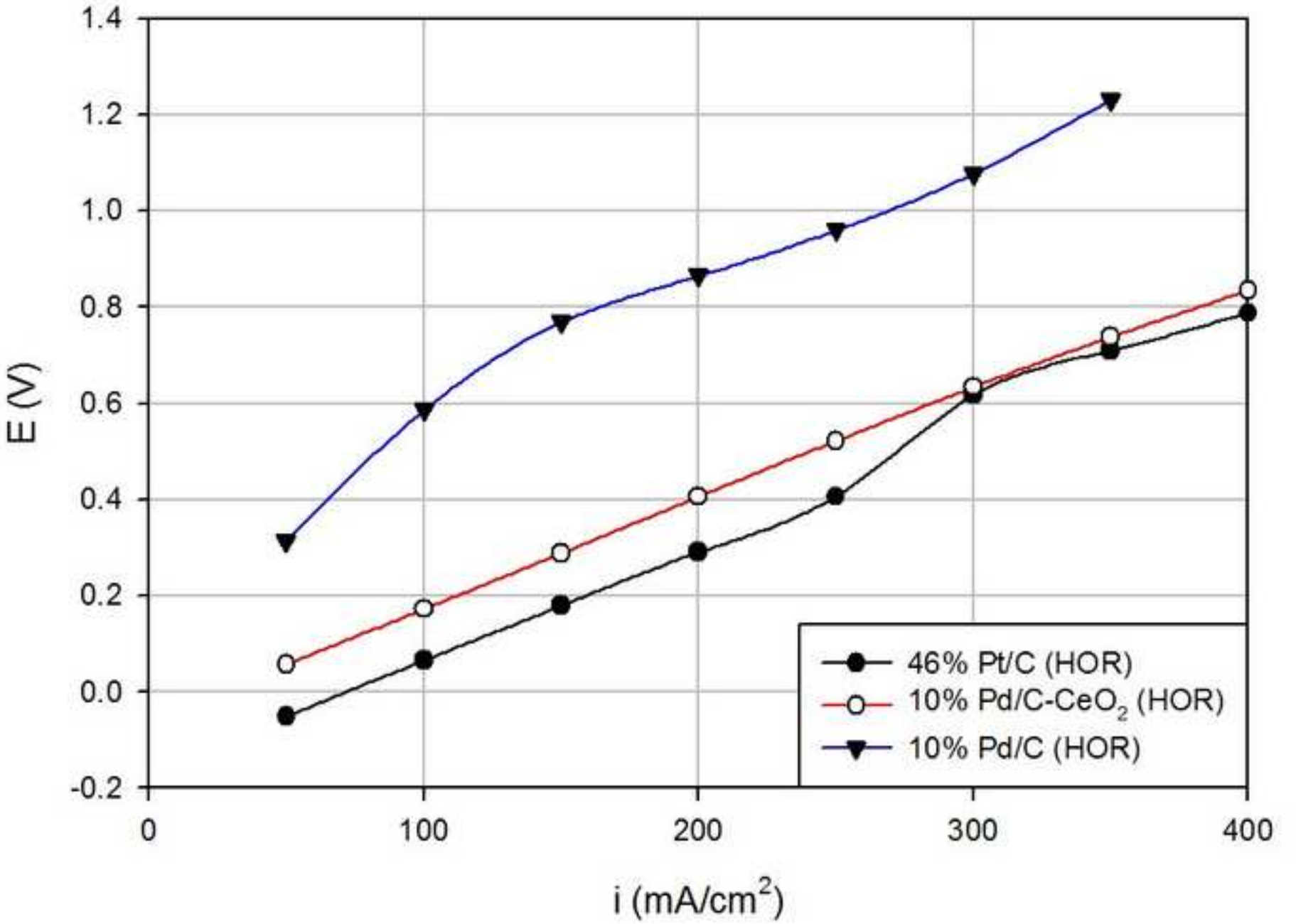

Figure 7

Click here to download high resolution image

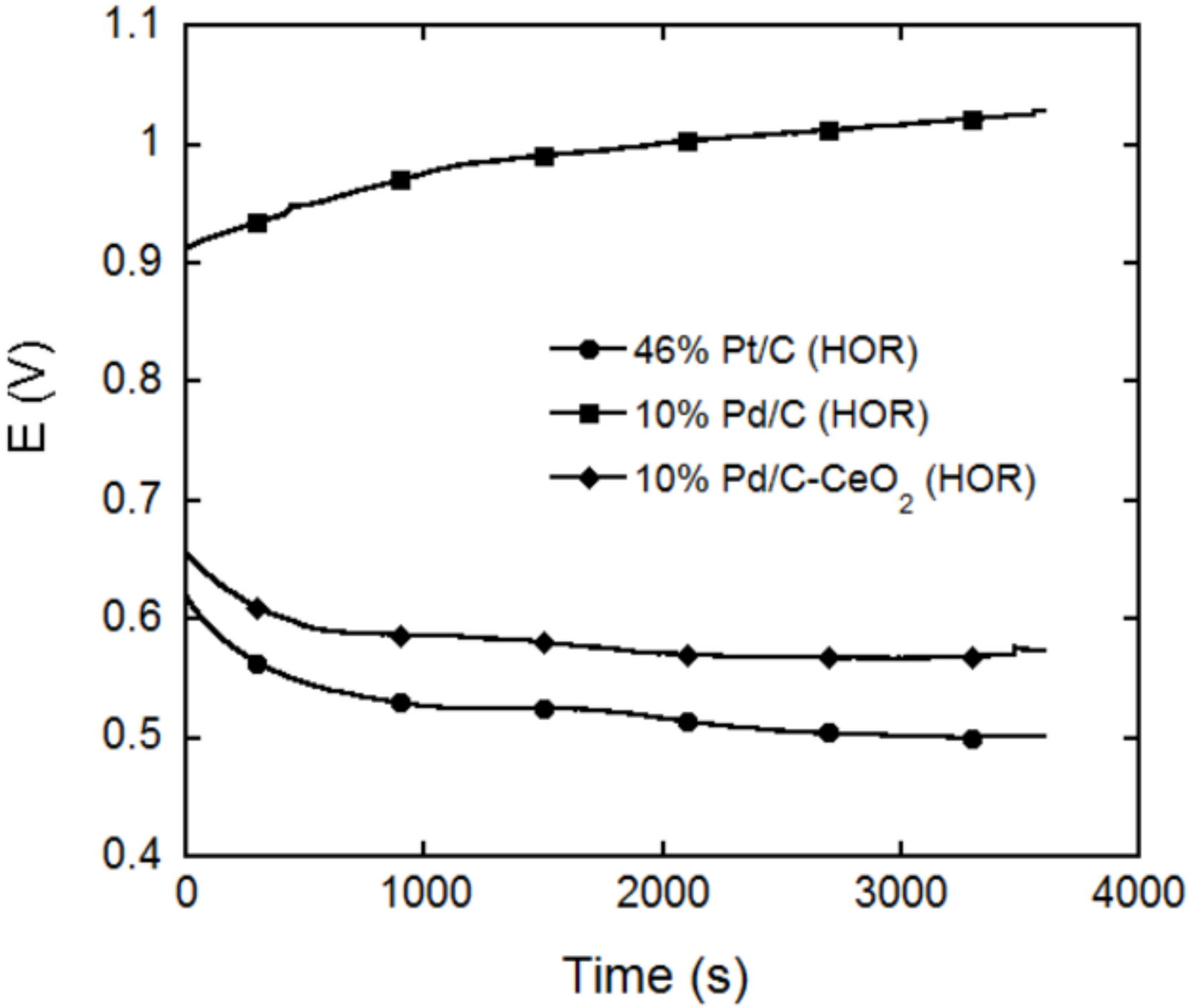

Figure 8

Click here to download high resolution image

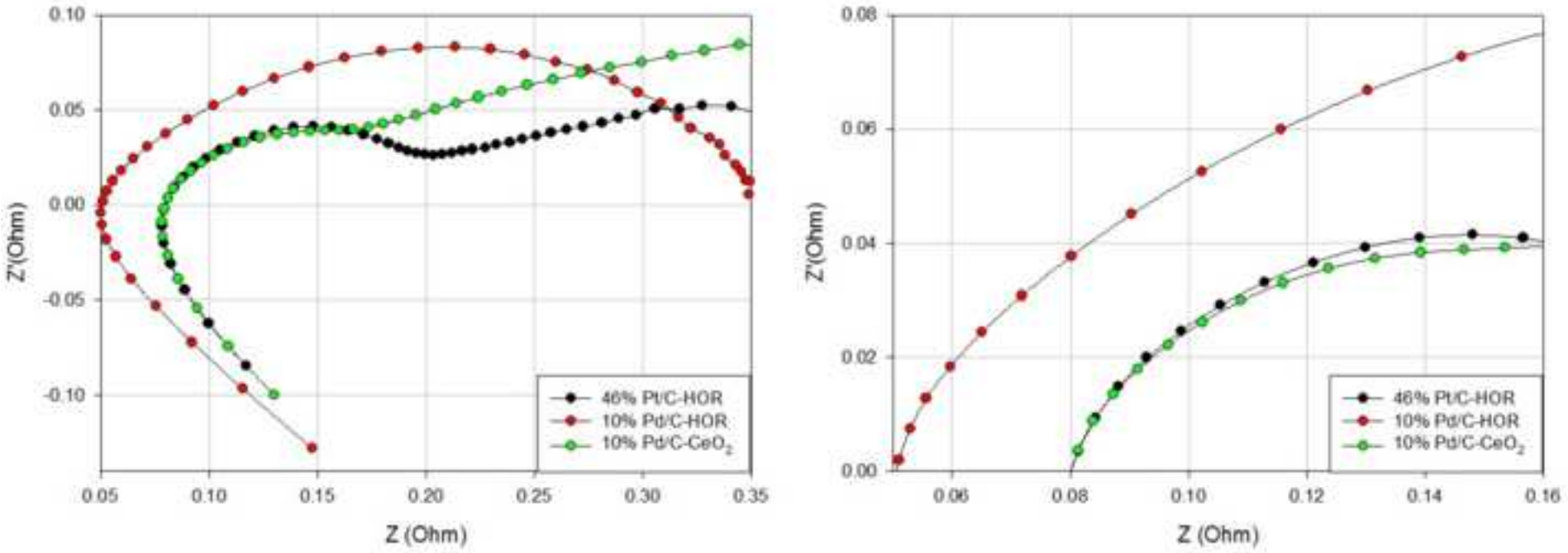

Figure 9

Click here to download high resolution image

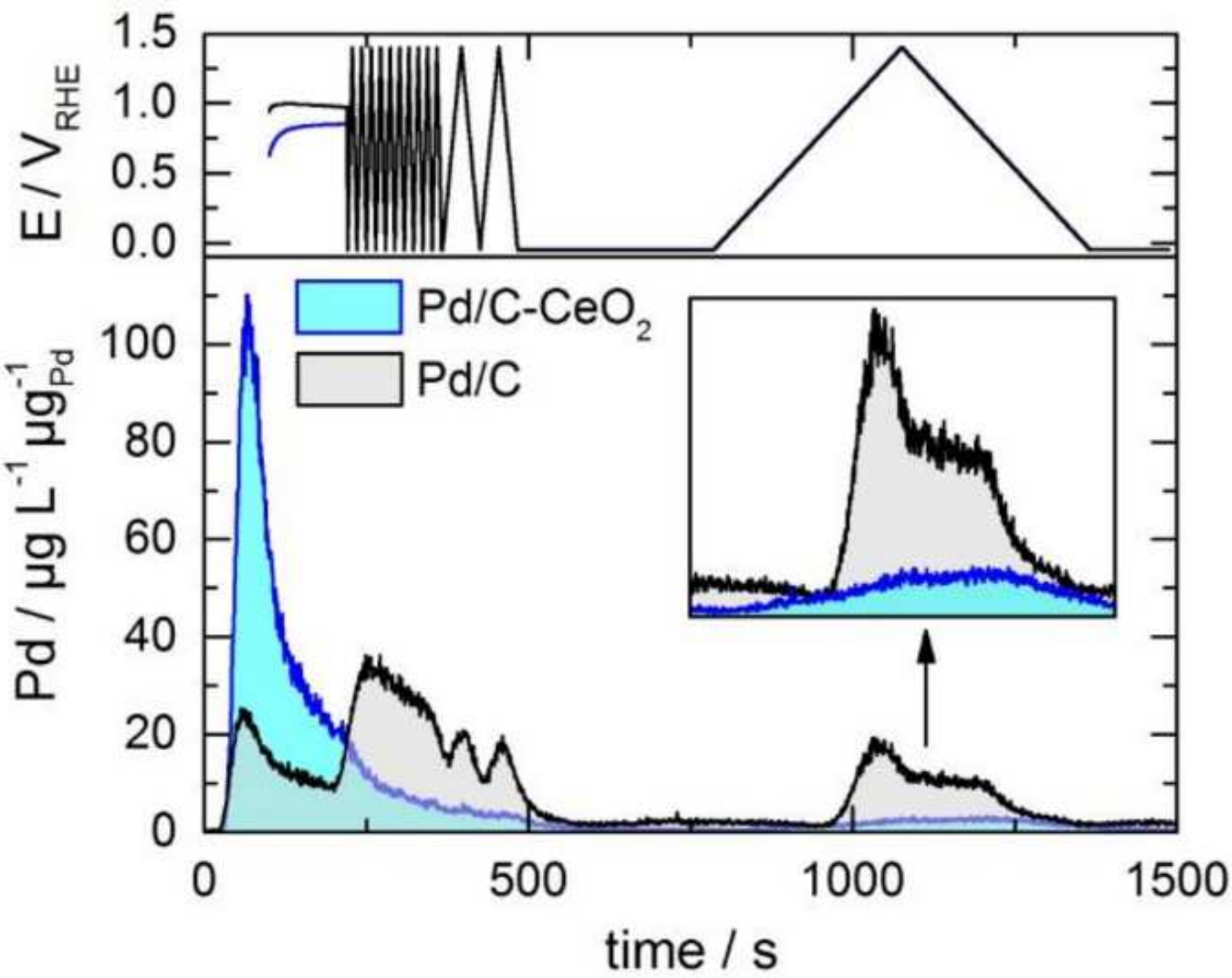

Figure 10

Click here to download high resolution image

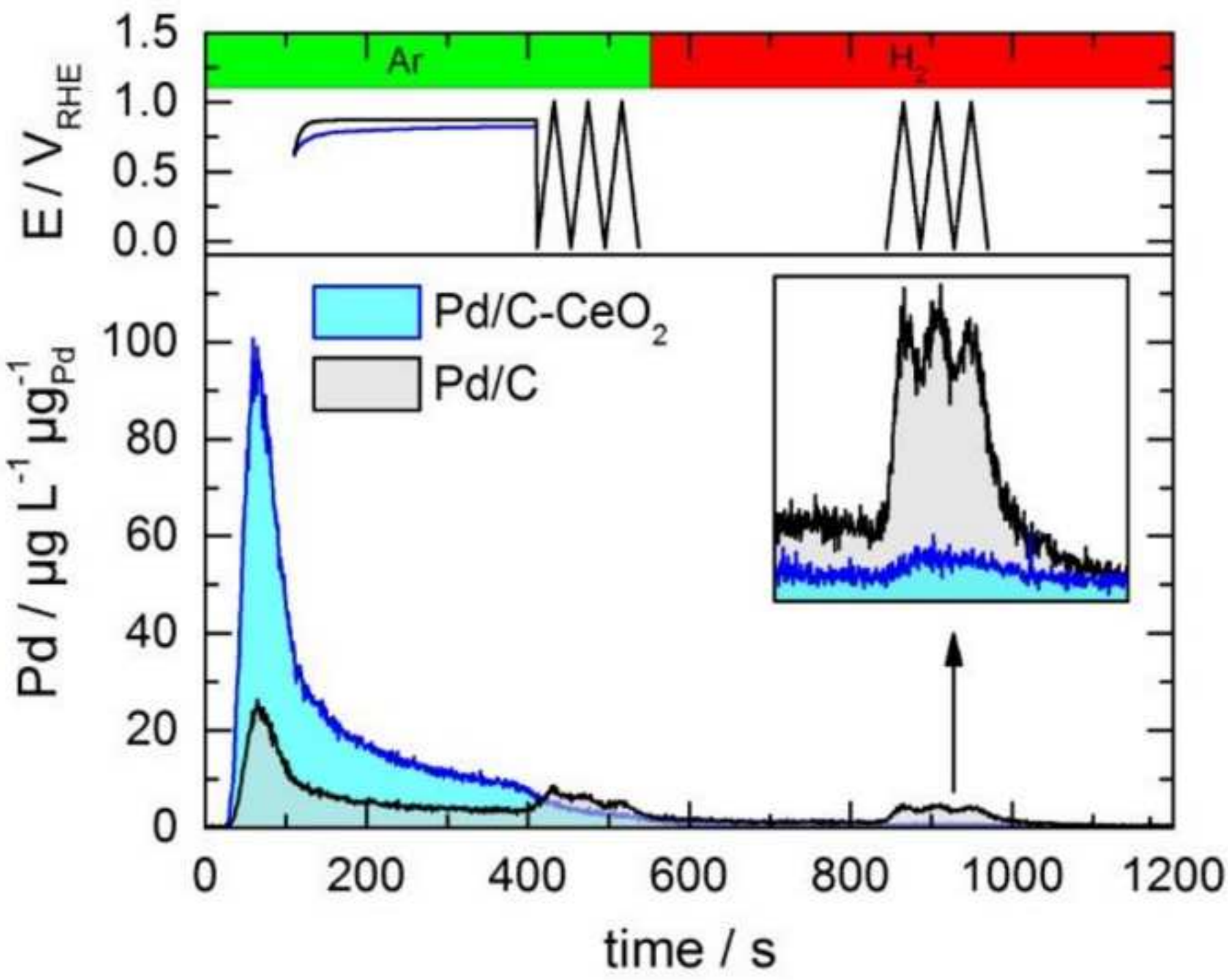

Figure 11

Click here to download high resolution image

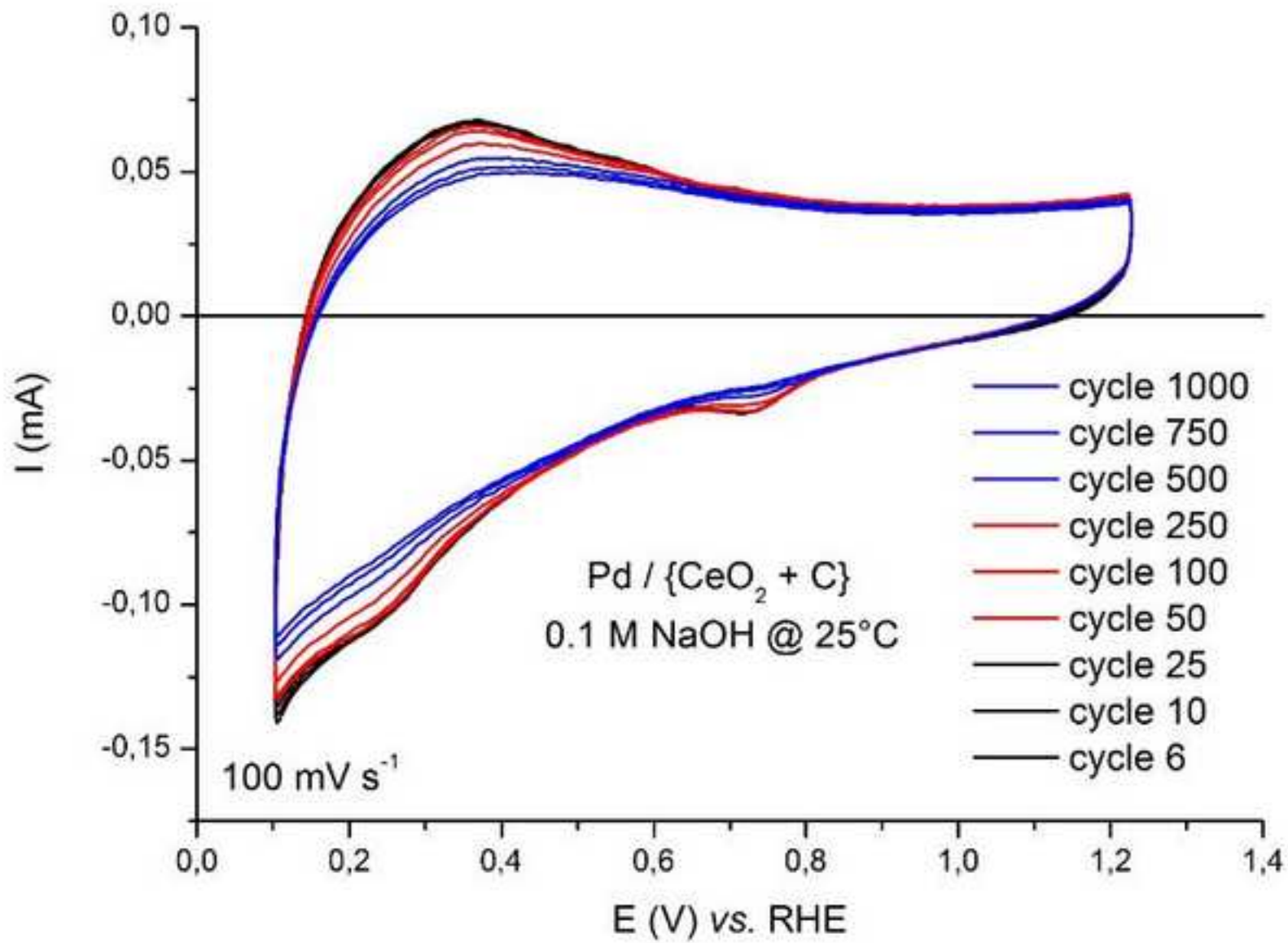

Figure 12

Click here to download high resolution image

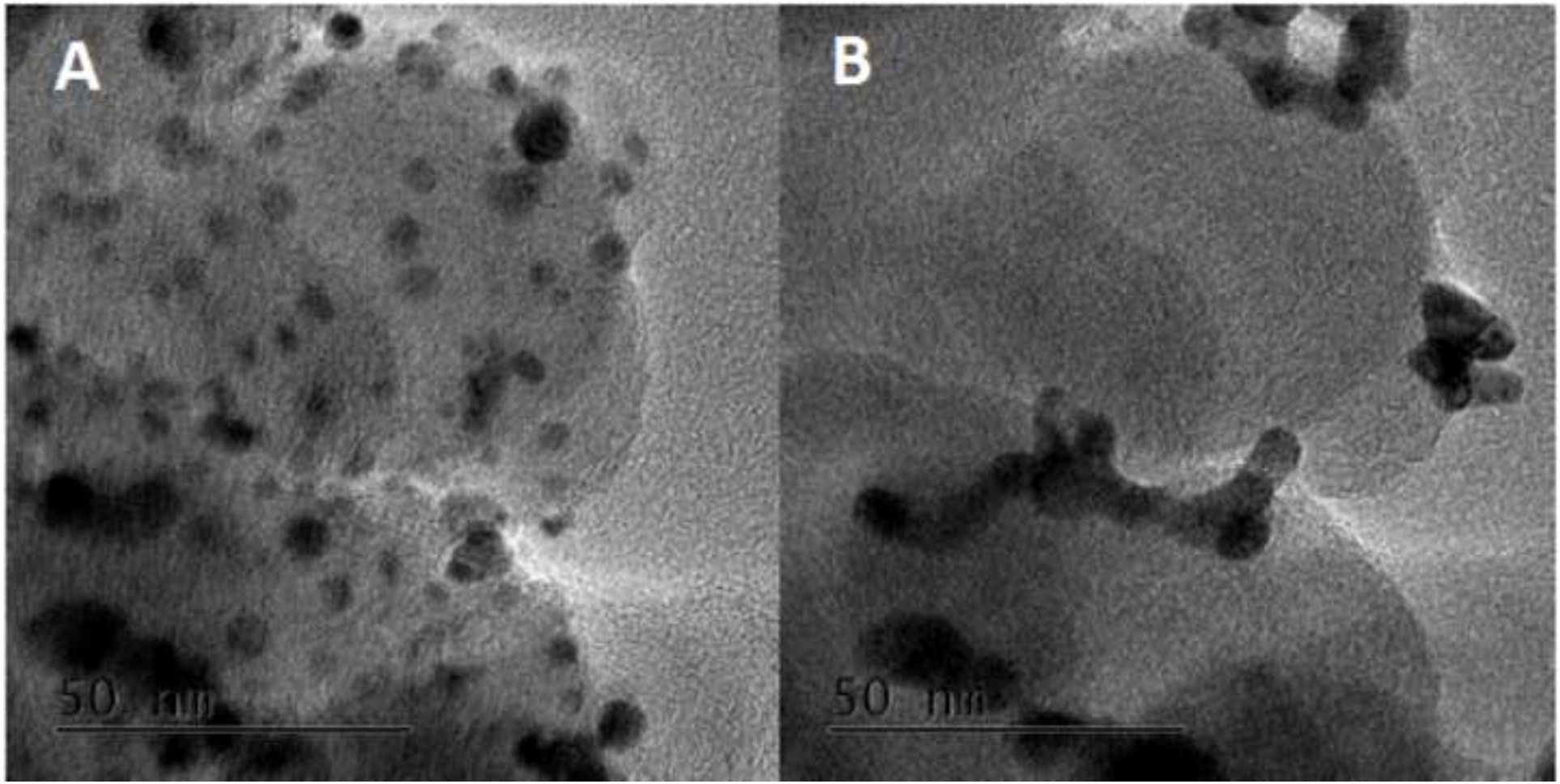

Figure 13

Click here to download high resolution image

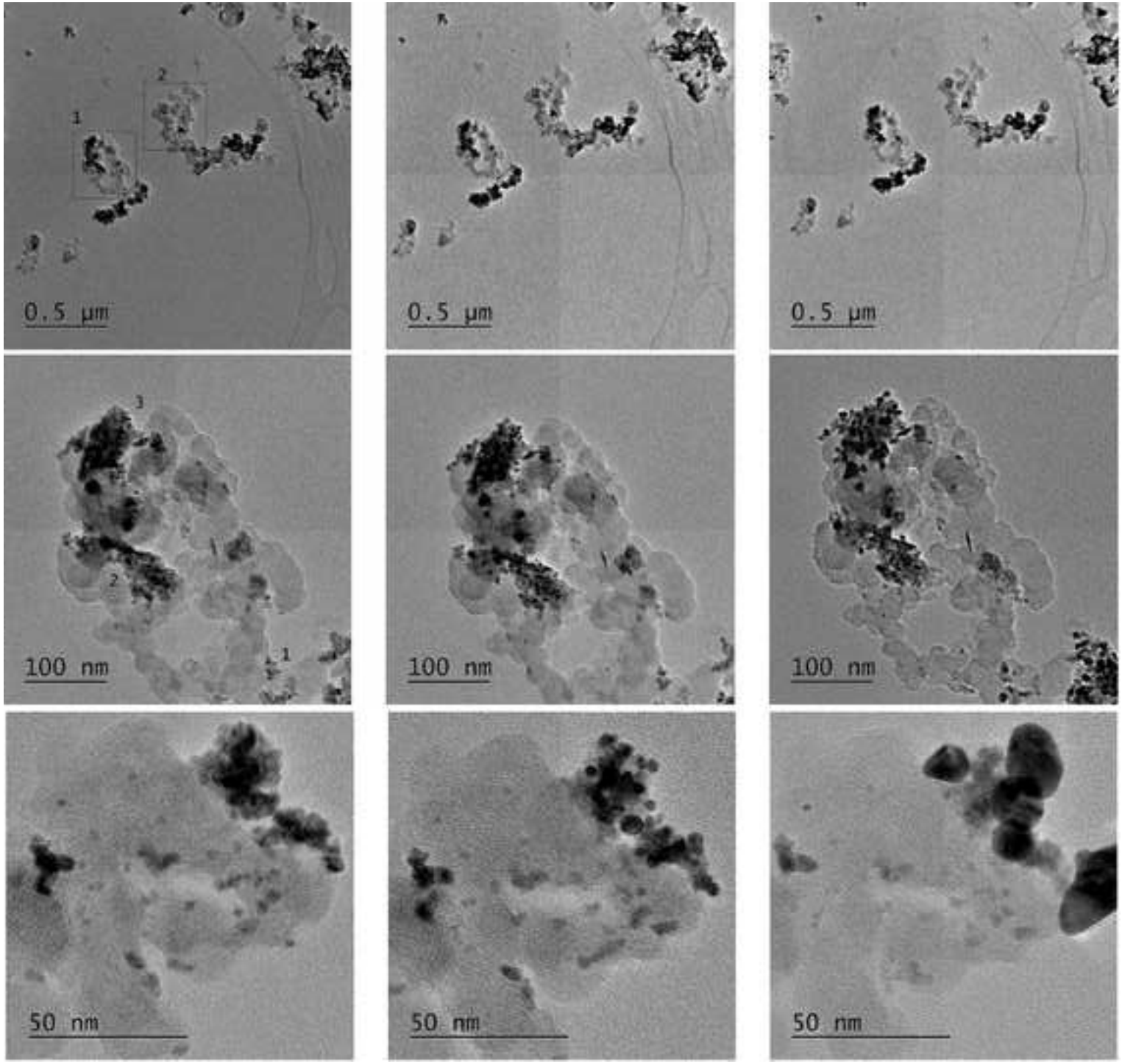

Figure 14

Click here to download high resolution image

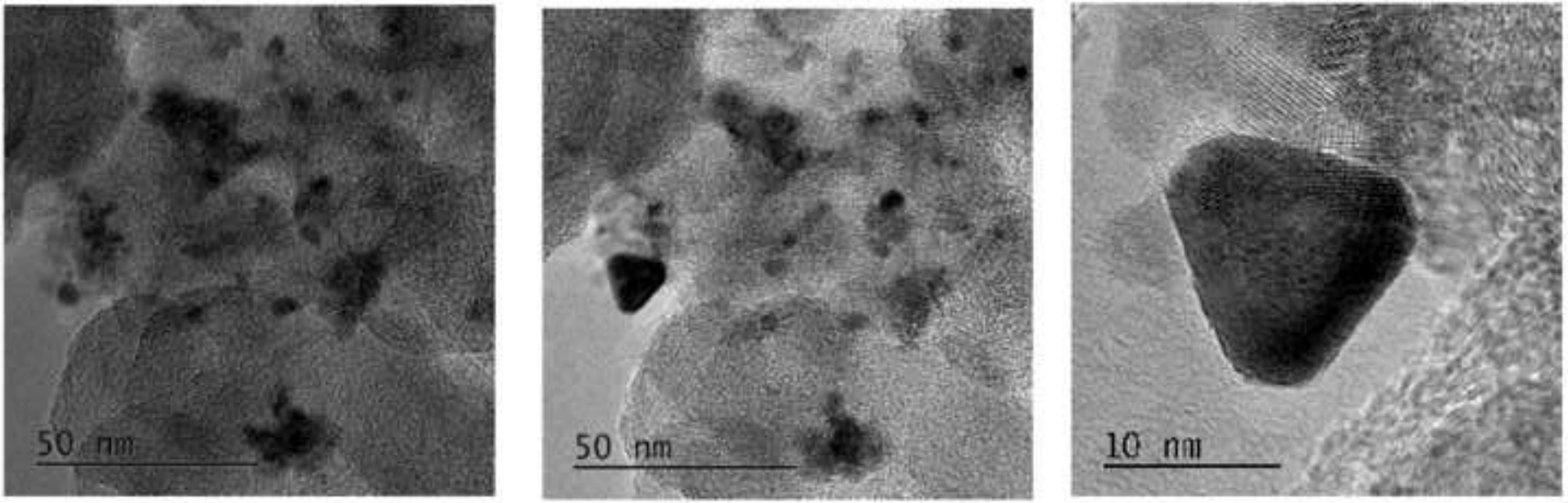

Supporting Information

Click here to download Supporting Information: Supporting info.docx

*Graphical Abstract